THE UNIVERSITY OF MICHIGAN
COLLEGE OF LITERATURE, SCIENCE, AND THE ARTS
Department of Physics

Technical Report

NEUTRON-PROTON, NEUTRON-DEUTERON, AND NEUTRON-NUCLEUS TOTAL CROSS SECTIONS AT 4.0 GeV/c AND 5.7 GeV/c

E. F. Parker
L. W. Jones

ORA Project 03028

supported by:

NATIONAL SCIENCE FOUNDATION
GRANT NO. GP-13265
WASHINGTON, D.C.

administered through:

OFFICE OF RESEARCH ADMINISTRATION ANN ARBOR

November 1969

This report was also a dissertation submitted by the first author in partial fulfillment of the requirements for the degree of Doctor of Philosophy in The University of Michigan, 1969.

ABSTRACT

Neutron total cross sections have been measured for H_2, D_2, He, Be, C, Al, Fe, Cu, Cd, W, Pb, and U at 5.7 ± 0.6 Gev/c incident momentum. The hydrogen and deuterium cross sections were also measured at 4.0 ± 0.6 Gev/c.

The deuteron screening factor was determined from the hydrogen and deuterium cross sections. The resulting values are compared with the previous experimental evaluations and theoretical predictions. The total cross section vs atomic number data were fitted to an optical model.

The experiment was performed at the Bevatron of the Lawrence Radiation Laboratory.

ACKNOWLEDGEMENTS

I would like to thank Professor Lawrence W. Jones for his continual guidance during the entire course of this experiment. His support and encouragement have been of inestimable value to me in my graduate studies.

I would like to express my gratitude to Professor Michael Longo and Dr. Bruce Cork for their invaluable contributions to the planning and performance of this experiment.

I am particularly indebted to Dr. H. Richard Gustafson, Fred Ringia, and Carl Cork for their help in the setting up and running of this experiment.

I am grateful to Bob Edwards, Walter Hartsough, and the entire staff of the Lawrence Radiation Laboratory Bevatron for the expert skill and cooperation so necessary to the successful setting up and running of this experiment.

It is with pleasure that I dedicate this thesis to my wife, Lois, whose faith, encouragement, and hard work made it possible.

TABLE OF CONTENTS

LIST OF TABLES

LIST OF FIGURES

LIST OF APPENDICES

CHAPTER I

INTRODUCTION

A. Objective

This thesis is a report of a neutral beam experiment performed at the Bevatron in the fall of 1968. Neutron total cross sections for twelve elements were measured at 5.7 Gev/c incident laboratory momentum. The total cross sections of two of the elements, hydrogen and deuterium, were also measured at 4.0 Gev/c. The deuteron screening factor and the charge independence of strong interactions were investigated as well as the atomic number dependence of neutron-nucleus total cross sections.

B. Summary of Previous Results

Proton-proton total cross sections have been measured at closely spaced momenta from 1 to 28 Gev/c[1-11] with generally good agreement among the various data sets. Proton-deuteron total cross sections have been measured[3,5,6,8,12] in this same momentum range. The agreement among the various data sets is generally good; however, there appears to be a systematic error in one of the two most extensive experiments[3,5] that causes the σ_t (pd) values of Bugg *et al.*[3] to be about 2 mb larger than the values of Galbraith *et al.*[5] The other pd measurements do not indicate which of these two data sets is incorrect as they are about equally divided in their agreement with these data.

The data on the neutron-proton total cross section above 1 Gev/c are limited to 15 points,[13-21] half of which lie below 4 Gev/c. The neutron-deuteron total cross section data are even more limited with only 8 points[12-19] above 1 Gev/c and only 4 points above 1.5 Gev/c.

The nucleon-nucleus total cross sections for a few elements have been covered reasonably well below 3 Gev/c[1,3,9,15,16,18,19,22] but the data above 3 Gev/c[21,23-26] are limited in extent and agreement. The results of the experiments of Atkinson et al.[21] at 6 Gev/c and Pantuyev et al.[24] at 8.3 Gev/c are in considerable disagreement with the trend of the other experimental results. The results of the 19 Gev/c proton measurement[25] and the 27 Gev/c neutron measurement[26] differ by 10% to 20%. This is difficult to understand in view of charge independence, and the slow variation of the nucleon-nucleon cross section in this momentum range. It is difficult to compare the results of Engler et al.[23] with other experiments since that experiment was performed with a neutron beam having a very broad momentum distribution. The authors specify their data as corresponding to a mean momentum of 10 Gev/c; however, the very wide momentum spread limits the value of this specification. Their data are in good agreement with the 19 Gev/c proton data;[25] however, with a factor of two difference between the specified momenta and the assumption of equal neutron and proton cross sections, one would expect the 10 Gev/c data to be about 5% higher, at least for the light elements, as is the case with the nucleon-

nucleon cross sections.

All of the data discussed in the above paragraphs are presented graphically in Chapter IV.

C. Theory

The deuteron cross section is equal to the sum of the np and pp cross sections minus a correction, δ, that, in the semiclassical view, allows for the eclipsing of one nucleon by the other in the deuteron; i.e.

$$\sigma(pd)=[\sigma(pp)+\sigma(np)][1-\delta] \qquad (1)$$

and

$$\sigma(nd)=[\sigma(nn)+\sigma(np)][1-\delta]. \qquad (2)$$

Glauber[27] has developed a model that considers the effects of elastic scattering in the "high energy limit" to estimate the size of this screening factor. He obtained the following approximate expressions:

$$\sigma(pd)=\sigma(pp)+\sigma(np)-\langle r^{-2}\rangle(1-\alpha_{np}\alpha_{pp})\sigma(np)\sigma(pp)/4\pi \qquad (3)$$

and

$$\sigma(nd)=\sigma(nn)+\sigma(np)-\langle r^{-2}\rangle(1-\alpha_{np}\alpha_{nn})\sigma(nn)\sigma(np)/4\pi, \qquad (4)$$

where α is the ratio of the real to imaginary part of the zero degree scattering amplitude and

$$\langle r^{-2}\rangle=\int S(\vec{q})\cdot Re[-f_{xn}(\vec{q})\cdot f_{xp}(\vec{q})]d^2\vec{q}/2\pi\cdot Re[f_{xn}(0)\cdot f_{xp}(0)] \qquad (5)$$

where $S(\vec{q})$ is the deuteron form factor, and the f's are the elastic scattering amplitudes at momentum transfer q. We

assume that the np scattering amplitude has the same form as the pp amplitude, and that the imaginary part of the scattering amplitude can be written as

$$\mathrm{Im}[f(q)]=\mathrm{Im}[f(0)]e^{-bq^2/2} \tag{6}$$

where q^2 is the four-momentum transfer squared. We also assume that the real part of the amplitude is proportional to the imaginary part of the amplitude for small q^2 so that

$$\mathrm{Re}[f(q)]= \alpha(0)\cdot\mathrm{Im}[f(q)] \ . \tag{7}$$

Experimentally, above 2 Gev/c, b is found to be a weakly momentum-dependent parameter. With these assumptions we can write

$$\langle r^{-2}\rangle = \frac{1}{2\pi}\int S(\vec{q})\cdot e^{-bq^2}\, d^2\vec{q} \ . \tag{8}$$

Table I lists values of $\langle r^{-2}\rangle$ calculated from Eq. (8) using a fit to the Gartenhaus wave function for the deuteron.[28] Since experimentally b is found to be between 6 and 10 $(\mathrm{Gev/c})^{-2}$ above 2 Gev/c, we conclude that $\langle r^{-2}\rangle$ is essentially constant above 2 Gev/c. Its calculated value is, however, dependent upon the assumed deuteron wave function. For example with a Hulthén wave function and a b of 9.6, Bugg et al.[3] derive a value of 0.034 mb^{-1}.

TABLE I

Theoretical Values of $\langle r^{-2} \rangle$ for Various Choices of b

b	$\langle r^{-2} \rangle$
2.0 $(GeV/c)^{-2}$	.031 mb^{-1}
4.0	.030
6.0	.028
7.0	.027
8.0	.027
10.0	.025
12.0	.022

If we combine Eq. (1) and (3) we get

$$\delta = \langle r^{-2} \rangle (1-\alpha_{np}\alpha_{pp})\sigma(pp)\sigma(np)/4\pi(\sigma(pp)+\sigma(np))$$
$$\approx \langle r^{-2} \rangle \sigma(pp)/8\pi \approx 1.6\langle r^{-2} \rangle mb \qquad (9)$$

since $\alpha_{np} \cdot \alpha_{pp} << 1$ [3,29] and $\sigma(np) \approx \sigma(pp) \approx 40mb$. We therefore conclude that the Glauber model predicts an energy-independent screening correction factor of about 0.05.

Pumplin and Ross[30] have expanded the Glauber model to include the screening effects associated with inelastic intermediate states of the incident nucleon. They conclude that the effects are not important below 5-10 Gev/c because of the coherence requirement that $kR \gtrsim 1$, where R is the radius of the nucleus, and k is the three-momentum transfer required to

produce an inelastic state of mass m with an incident laboratory momentum K, i.e. $k \gtrsim m^2/2K$. Above 5-10 Gev/c the effect should increase with energy, yielding a decrease in the $\sigma(pd)$ cross section of 1.8 mb at 30 Gev/c. This translates into an increase in δ from about 0.05 below 5-10 Gev/c to $\delta \gtrsim 0.06$ at 30 Gev/c.

The total cross sections of more complex muclei can also be expressed in terms of the nucleon-nucleon cross sections, i.e.

$$\sigma(pA)=[(A-Z)\sigma(np)+Z\sigma(pp)][1-\delta] \qquad (10)$$

and

$$\sigma(nA)=[(A-Z)\sigma(pp)+Z\sigma(np)][1-\delta] \qquad (11)$$

assuming charge symmetry [$\sigma(nn)=\sigma(pp)$]. As in the deuterium case, δ allows for the elastic and inelastic shadow effects. Pumplin and Ross[30] have also calculated these effects for A=9,64, and 207 and conclude that inelastic effects are insignificant below 5-10 Gev/c but can give δ a significant energy dependence above 10 Gev/c. Specifically they calculate a 50% increase in δ for Be at 30 Gev/c relative to its low momentum value. They predict an increase of about 10% in δ for Pb.

D. Report Outline

The scheme of this report is as follows: Chapter II contains a detailed description of the experimental apparatus and set-up, Chapter III discusses the data analysis and the various correction factors that had to be considered and

Chapter IV discusses the results in terms of a simple absorption model and also compares them with most of the available nucleon total cross section measurements above several hundred Mev. The deuteron and nuclear screening factors are also evaluated and compared with the theoretical predictions.

CHAPTER II

EXPERIMENTAL SETUP AND APPARATUS

A. Experimental Arrangement

Fig. 1 is a diagram of the experimental layout on the floor of the Bevatron. The neutron beam was produced in a 6 in. x 1/4 in. x 1/4 in. Be target mounted in the Bevatron vacuum tank and was defined by a 10 ft. length 5/8 in. diameter collimator located in the shield wall. Charged particles were removed from the beam by the large C-type (36 in. pole length) electromagnet located just downstream of the machine port, and a small (24 in. pole length) permanent magnet located just downstream of the defining collimator. The large magnet had a field strength of about 20,000 gauss and the permanent magnet had a strength of about 1200 gauss. In order to reduce the background radiation near the monitor counters, the magnet gap was filled with lead except for a 4 in. x 4 in. tunnel along the beam line, and a 5 ft. x 1 ft. x 6 in. Pb block with a 1 in. diameter collimator was located just upstream of the magnet. A 1 in. diameter, 5 ft. length collimator was placed downstream of the defining collimator to minimize any halo from scattering off the collimator walls. The solid targets, i.e. Be-U, were mounted on a platform located where the beam exits from the shield wall, and the liquid target was located 2 ft. downstream of the shield wall. The transmission counters and the calorimeter assembly were mounted on a cart and track that allowed the target-calorimeter

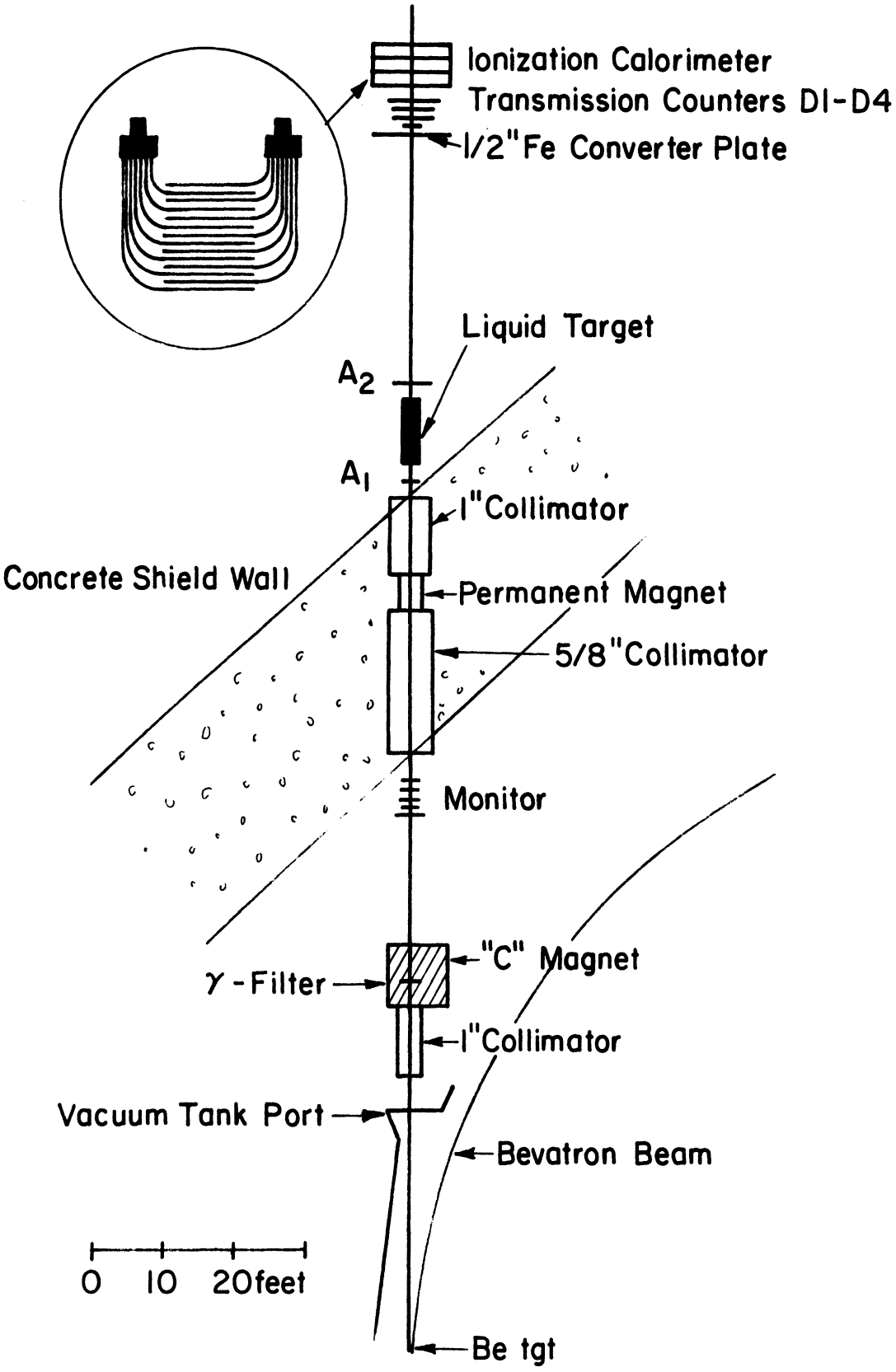

Fig. 1 Experimental Layout

separation to be varied by about 20 ft. This feature was included primarily for utilization in a small angle elastic scattering experiment that followed this total cross section experiment. For this experiment the converter plate-solid target position separation was 313.5 in. and the distance between the converter plate and the center of the liquid target was 262.5 in. The beam monitor was located in the beam just upstream of the shield wall and consisted of a 1/2 in. thick block of CH_2 viewed by a three counter telescope.

Specific details of these various components are given in the following paragraphs.

B. Beam

The beam line was at an angle of 2.5 degrees relative to the proton beam direction at the Be target. The distance between the Be target and the center of the defining collimator was 575 in. and the distance from the collimator center to the converter plate was 480 in. The beam was 1.12 in. in diameter at the converter plate and had no noticeable halo.

The momentum distribution of the beam was not measured in this experiment; however, the small angle neutron spectrum from Be has been measured under quite similar circumstances[31] and was found to be well represented by an empirical fit to the data on the production of inelastic protons by protons on Be;[32] i.e.

$$\frac{d^2N}{dpd\Omega}=p^2\left[1.0+\frac{0.47P_b}{P^2}\right]\left[\frac{0.56}{P_b}+\frac{0.44}{P_b^2}\,P\left(1.0-\frac{0.47P_b}{P^2}\right)\right]e^{-3.0(p\theta)^2} \tag{12}$$

where P_b is the momentum of the incident beam, and θ is the production angle. The beam intensity was typically about 2 to 5 x 10^4 neutrons per spill.

A small γ-ray contamination can produce a significant error in the total cross section, and great care was taken to assure that there was no significant γ-ray component. This was accomplished by measuring the attenuation cross section for a 0.625 in. thick Pb target as a function of γ-ray filter (Pb) thickness. The radiation length in lead is much shorter than the nuclear collision length; therefore, the beam attenuation factor for the 0.625 in. Pb target will be strongly dependent upon the γ-ray to neutron ratio. This ratio is strongly dependent on the amount of filtration. When it has been reduced to a negligible value, the beam attenuation factor will become independent of the filter thickness. The resulting data are shown in Fig. 2. On the basis of these data a 3 in. lead filter was placed in the beam at the sweeping magnet.

C. Beam Monitor

The beam monitor and its associated logic are shown in Fig. 3. The anticounter was a 2 in. x 2 in. x 1/2 in. scintillator mounted on a 6810A PM tube and the three counters in the telescope were 1.25 in. x 1.25 in. x 0.125 in.

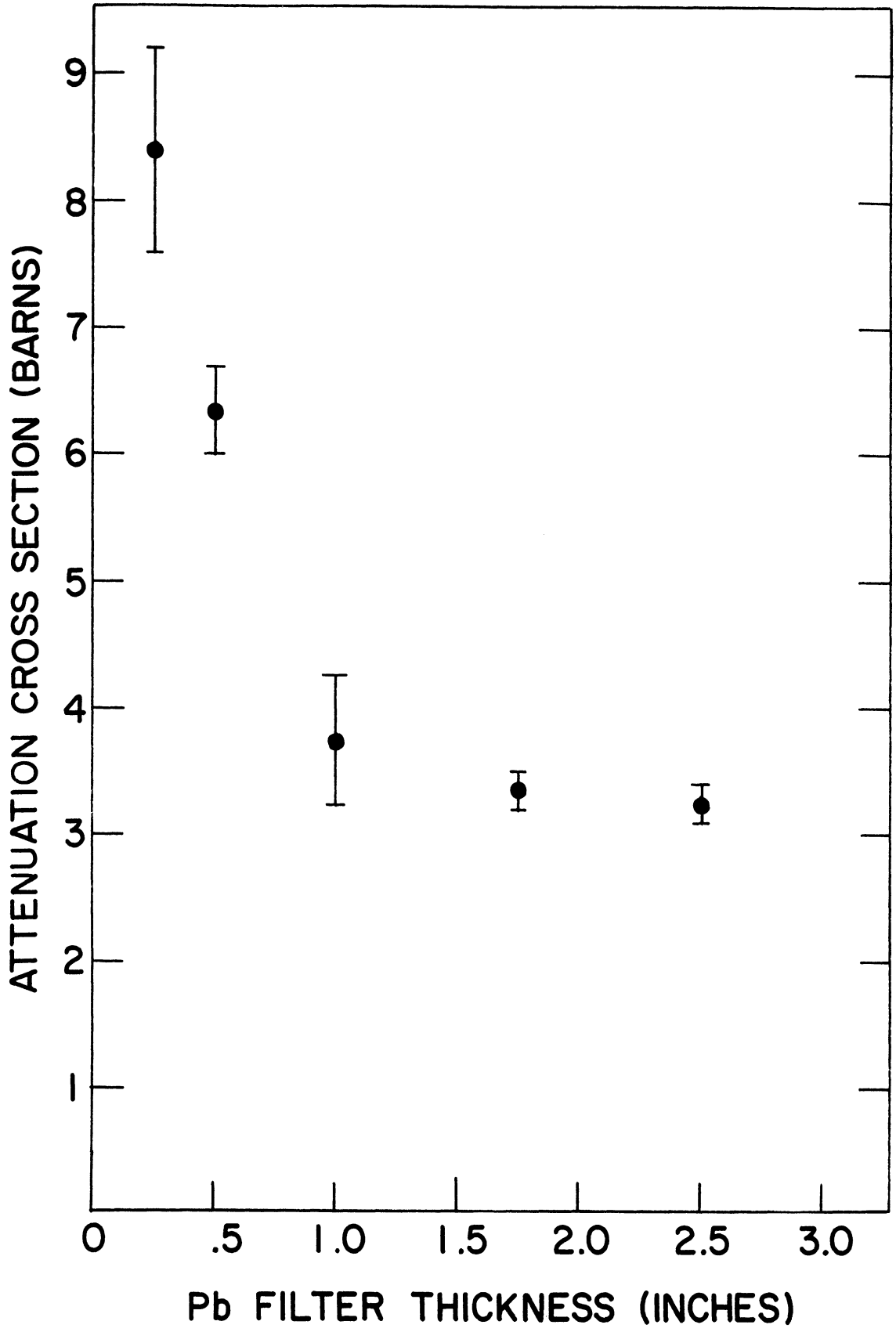

Fig. 2 Attenuation Cross Section for 0.625 in. Pb Target as a Function of γ-Ray Filter Thickness

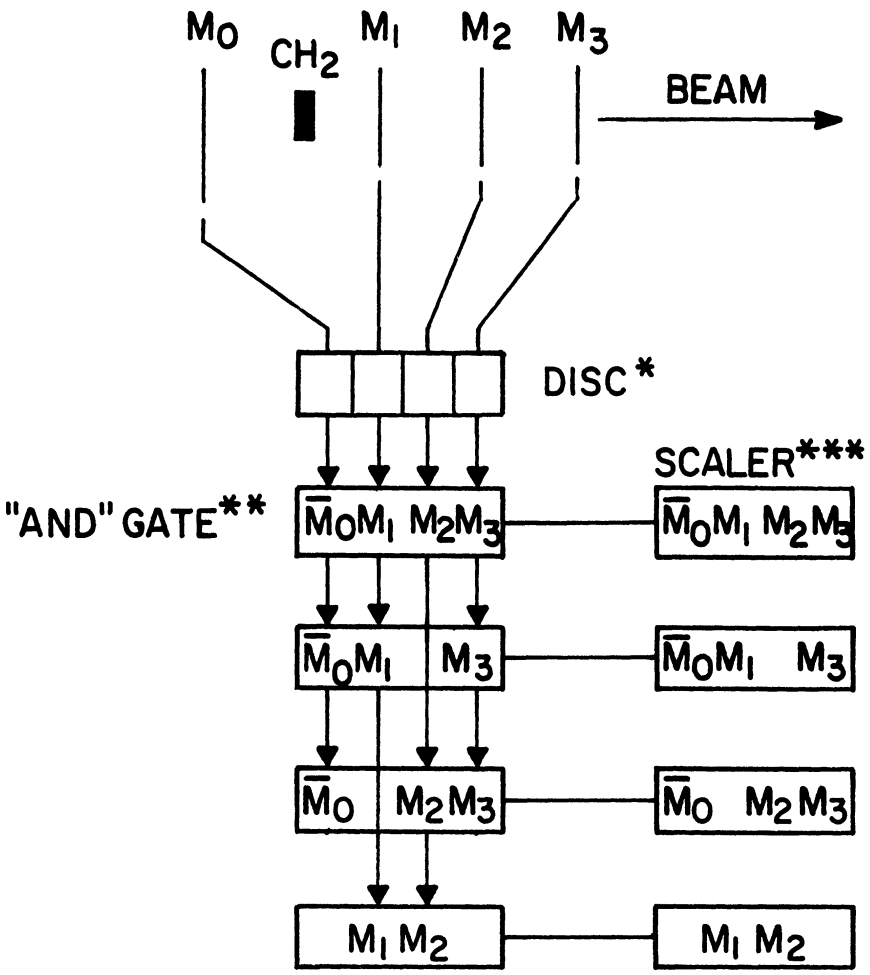

* Chronetics 104 Quad Disc.

** All "And"Gates were Chronetics Model 113's

*** All Scalers were LRL "Jackson" Scalers

Fig. 3 Beam Monitor Diagram

scintillators mounted on 53AVP PM tubes. The converter was a 0.5 in. thick by 1.5 in. diameter CH_2 disc. A very small fraction ($\sim$1%) of the incident neutrons interacted in the CH_2 converter and produced a forward-going spray which was detected in the telescope, thereby giving a count rate directly proportional to the incident neutron intensity. The anticounter was used to assure that the monitor was counting incident neutrons and not charged particles. Although $M_1 \cdot M_2 \cdot M_3 \cdot \bar{M}_o$ was the primary monitor, the various double coincidences were scaled and recorded to have a continuous check on the stability of the monitor counters. Counter instabilities were negligible throughout the experiment.

D. Transmission and Anticoincidence Counters

Anticoincidence counters were located just upstream and downstream of the targets. The upstream counter was a 1.5 in. x 1.5 in. x 1/16 in. scintillator mounted on a 6810A PM tube and was used to veto events due to any charged particles in the beam. The downstream counter was a 4 in. x 4 in. x 1/16 in. scintillator mounted on a 6810A PM tube and was used to veto events due to charged particles coming out of the target.

The four transmission counters were 0.25 in. thick discs having 1.5 in., 2.5 in., 4.5 in., and 7.75 in. diameters and mounted on 6810A PM tubes. They were mounted in series between the converter plate and the body of the calorimeter as shown in Fig. 4. The axes of the counters were coincident with the beam center line to within 0.1 in. The two smallest

counters were fitted into 0.25 in. thick lucite sheets so that regardless of where a neutron hit a counter, it had previously passed through the same amount of material. The 4.5 in. counter light pipe was large enough to cover the 7.75 in. counter. The solid angles and mean $|t|$ (four-momentum transfer) ranges subtended by these four counters relative to the geometric centers of the liquid and solid targets are given in Table II.

TABLE II

Transmission Counter Solid Angles

Counter Diameter (inches)	Solid Angles (sterad.)		Mean t Range $(Gev/c)^2$		
			liquid		solid
	liquid	solid	5.7Gev/c	4.0Gev/c	5.7Gev/c
D4-1.5	2.6×10^{-5}	1.8×10^{-5}	2.2×10^{-4}	1.1×10^{-4}	1.6×10^{-4}
D3-2.5	7.1×10^{-5}	5.0×10^{-5}	7.5×10^{-4}	3.7×10^{-4}	5.1×10^{-4}
D2-4.5	2.3×10^{-4}	1.6×10^{-4}	2.5×10^{-3}	1.3×10^{-3}	1.8×10^{-3}
D1-7.75	6.8×10^{-4}	4.8×10^{-4}	7.8×10^{-3}	4.0×10^{-3}	5.5×10^{-3}

E. Ionization Calorimeter

The calorimeter[1] consisted of 14 aluminum plates interleaved with scintillators as shown in Figs. 4 and 5. The scintillators were 32 in. x 22 in. x 0.25 in. sheets of Pilot Chemical Co. type F plastic scintillator. The scintillators were divided into two interleaved groups of seven which were summed optically and viewed by an RCA 4522 PM tube, a 5 in.

---

[1] Discussions on the theory and applications of calorimeters are given in Ref. 33 and 34.

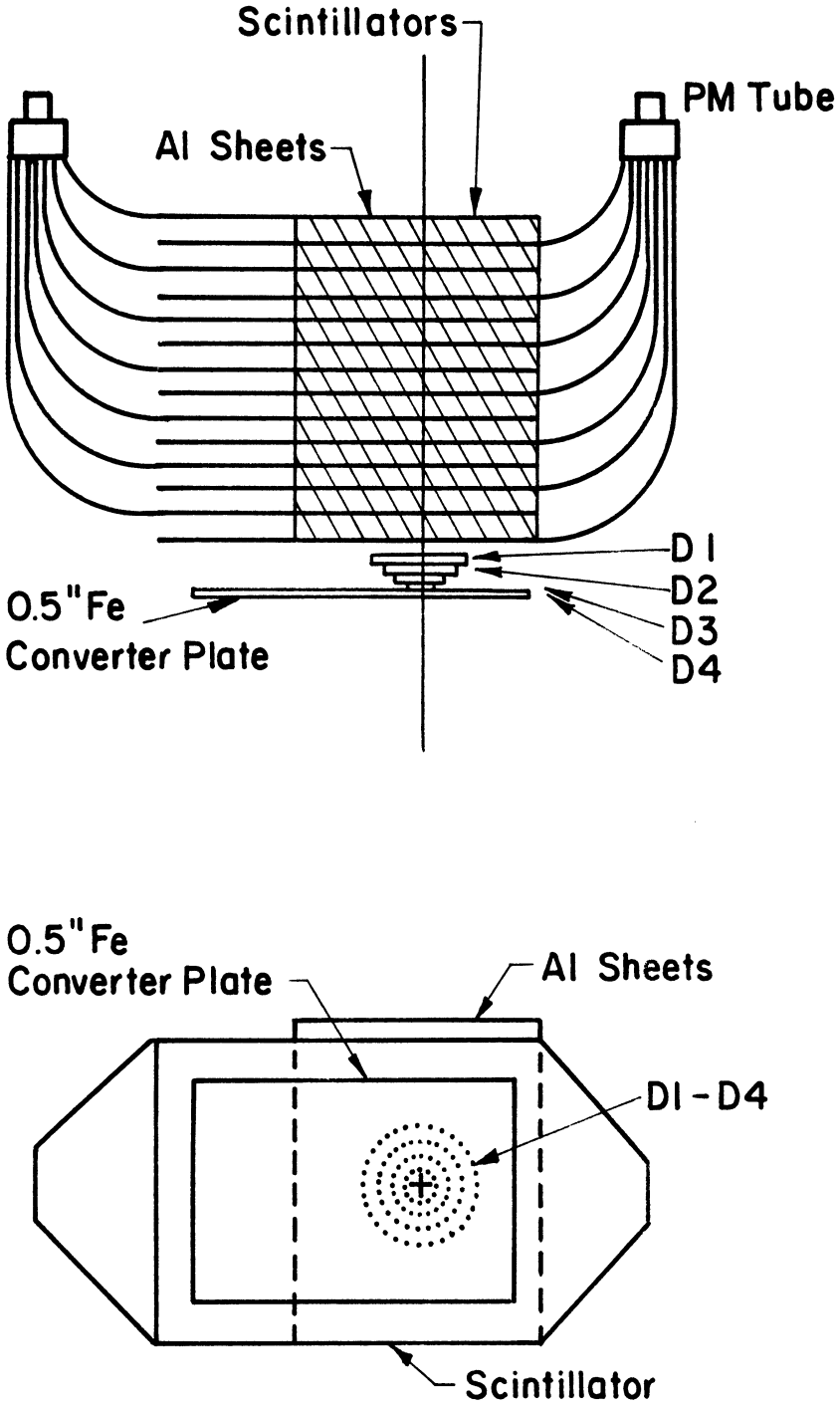

Fig. 4 Ionization Calorimeter and Transmission Counter Assembly

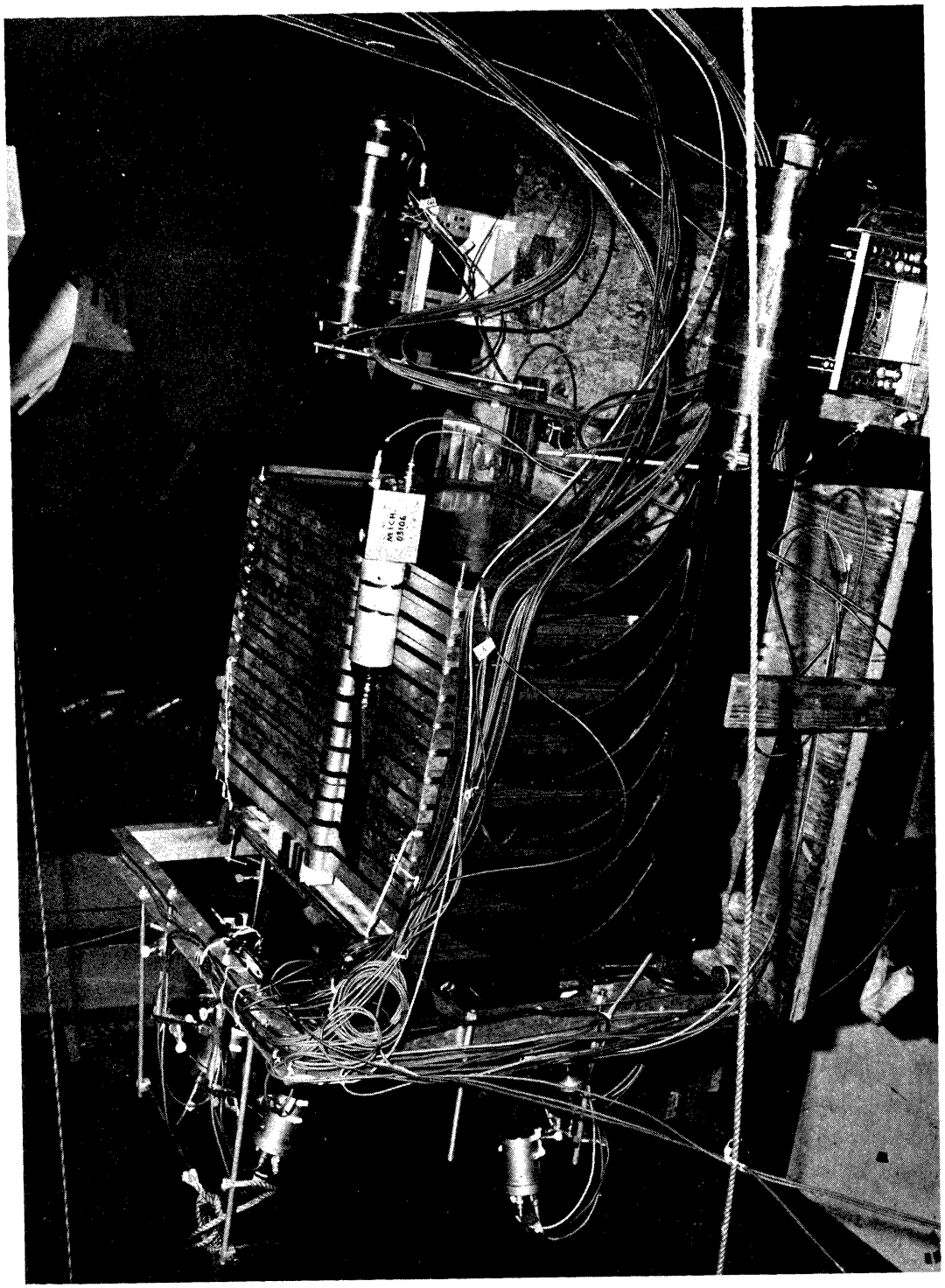

Fig. 5 Ionization Calorimeter

diameter, 12 stage tube with a bialkali photocathode. The outputs of the two PM tubes were passively summed. The Al sheets were 19 in. x 19 in. x 1.25 in. The original design called for Fe instead of Al absorbing layers; however, an experimental evaluation showed that Al yielded a slightly better resolution than Fe at Bevatron energies.

The response characteristics of the calorimeter are discussed in Appendices I, II, III, and IV.

F. Electronics

Fig. 6 is a diagram of the electronics for this experiment. The labels "50% Cal" and "10% Cal" signify that the input attenuation for the two calorimeter discriminators was such that only the upper 50% and 10% of the calorimeter output pulses could trigger their respective discriminators. The effective neutron spectra for these two attenuation levels are shown in Appendix I. The largest transmission counter, D1, was in coincidence with the 10% Cal and in anticoincidence with the anticounters. The Cal(10%)·D1·$\overline{A}$ output was then put in coincidence with the 4.5 in. disc counter, D2. This output in turn was put in coincidence with the 2.5 in. disc counter, D3, and finally this output was connected in coincidence with the 1.5 in. disc counter, D1. This coincidence cascade was duplicated for the 50% Cal. The 50% calorimeter was included primarily as a check on the operation of the 10% logic and as a convenience for making various tests during data runs.

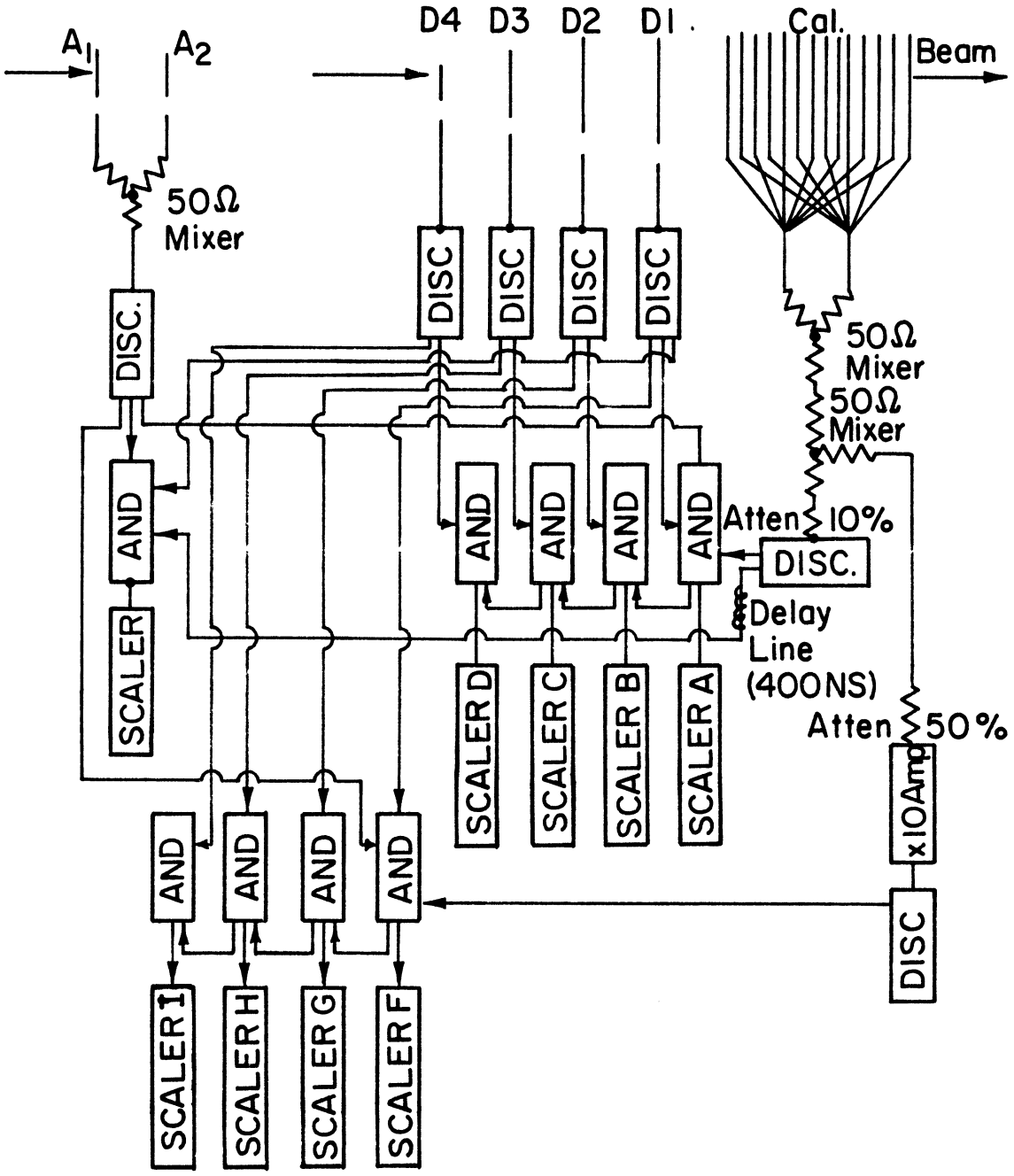

Scaler A = Cal(10%)·D1·$\bar{A}$
" B = Cal(10%)·D1·D2·$\bar{A}$
" C = Cal(10%)·D1·D2·D3·$\bar{A}$
" D = Cal(10%)·D1·D2·D3·D4·$\bar{A}$
" E = Delayed Cal(10%)·D1·$\bar{A}$
" F = Cal(50%)·D1·$\bar{A}$
" G = Cal(50%)·D1·D2·$\bar{A}$
" H = Cal(50%)·D1·D2·D3·$\bar{A}$
" I = Cal(50%)·D1·D2·D3·D4·$\bar{A}$

Note: All Disc. are Chronetics Model 101.
All "And" Gates are Chronetics Model 113.
Scalers A-D are Trans. Spec. Inc. model 1511.
Scalers E-I are LRL "Jackson" Scalers.

Fig. 6 Electronics Diagram

The "delayed Cal(10%)·D1·$\overline{A}$" coincidence was included to give a continuous measure of the accidentals rate and also an indication of the instantaneous beam intensity for making rate corrections on the data (see Appendix II). The delay-line length was equal to one period of the Bevatron RF system, i.e. about 400 ns.

The scaler data were typed out and punched on paper tape at the end of each run. For the solid targets a complete in-out sequence was limited to about 10 minutes with about 30 seconds required to record the data and change the target. For the liquid targets the sequence was extended to about 20 minutes because of the longer time required ($\sim$3 minutes) to change the target state. These short cycle times were used to minimize the effects of any temporal drifts in the equipment. One such variation was caused by temperature changes in the calorimeter discriminator. Although the Chronetics logic is relatively temperature-insensitive, small temperature-induced changes in the triggering level coupled to a very steep pulse height spectrum (see Fig. A-1) were found to produce significant effects in the 10% calorimeter count rate relative to the monitor. For this reason great care was taken to avoid short-term temperature changes in this discriminator, and, the discriminator temperature was continually monitored and displayed on a strip-chart recorder.

G. Targets

The liquid target is sketched in Fig. 7. The flask

was emptied for the target "out" runs by closing the flask vent and increasing the pressure above the liquid by adding helium gas to force the liquid into the reservoir. The target "out" runs for liquid hydrogen were therefore not actually with an empty flask but rather with the flask filled with a gaseous helium and hydrogen mixture at one atmosphere. Helium was also used to empty the flask in the liquid helium runs; however, deuterium gas was used for the liquid deuterium runs. In the liquid hydrogen and liquid helium runs the flask vent was opened to the atmosphere; however, in the liquid deuterium runs a closed-loop arrangement was required to avoid loss of the deuterium. Since the deuterium was condensed from the gaseous state by passing it over a condenser at LH_2 temperature, the LD_2 system equilibrium pressure was 0.5 atmospheres. Helium was added to the system to bring the pressure up to 0.75 atmospheres. Although it would have been quite helpful to have been able to measure the temperature of the gas in the flask during the target "out" runs, repeated attempts to do so failed.

As stated above, the flask was 48 in. long at room temperature with no pressure inside. However, this length must be corrected for the expansion produced by the pressure differential (1 atmosphere) and the contraction produced by the temperature reduction from essentially 300 degrees K to 20 degrees K. The following correction factors were obtained from the Lawrence Radiation Laboratory mechanical engineering group:[35]

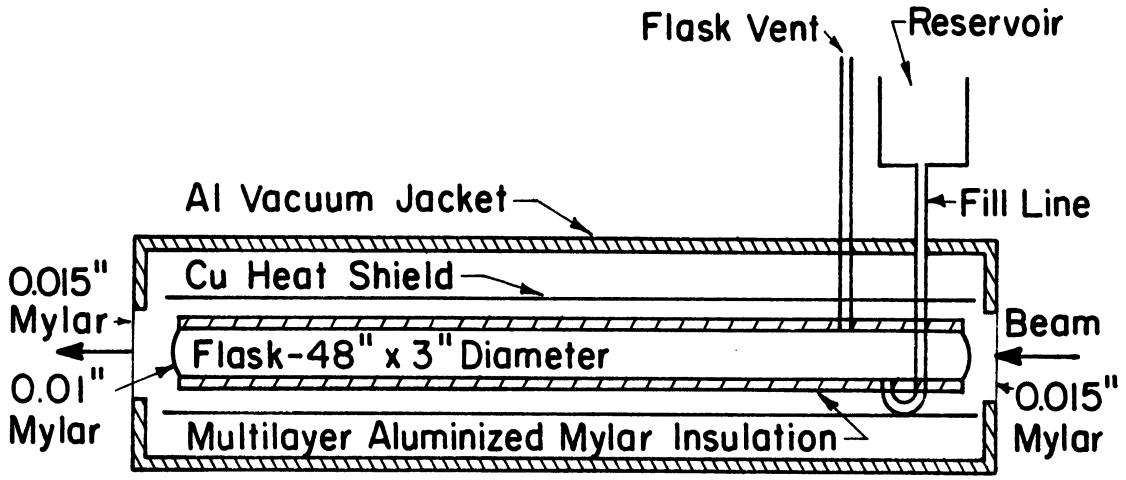

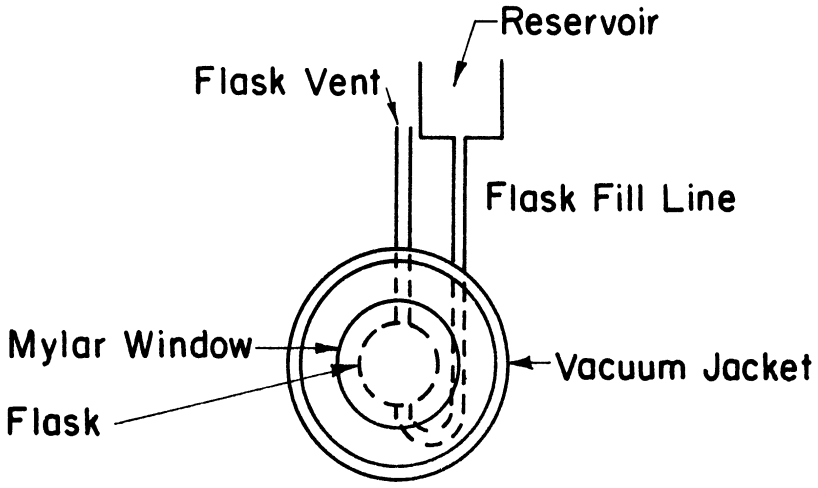

Fig. 7 Liquid Target

thermal contraction 0.155 inches

pressure expansion 0.350 inches/atmosphere.

The corrected flask lengths are 48.195 in. for the liquid hydrogen and helium runs and 48.11 in. for the liquid deuterium runs.

The temperature of the liquid hydrogen and deuterium was determined by the liquid hydrogen boiling at one atmosphere in the reservoir. This resulted in a density of 0.0707 $\pm$ 0.0001 g cm^{-3} for hydrogen[36] and 0.1708 $\pm$ 0.0003 g cm^{-3} for deuterium.[37] The liquid helium temperature was determined by the liquid helium boiling at one atmosphere resulting in a density of 0.1255 g cm^{-3}.[38]

The physical characteristics of the solid targets are given in Table III.

TABLE III

Solid Target Properties

Element	Thickness (inches)	Density (g cm^{-3})
Be	3.690	1.854
C	3.000	1.768
Al	3.012	2.77
Fe	0.9922	7.871
Cu	1.000	8.974
Cd	1.663	8.65
W	0.9233	19.3
Pb	1.504	11.34
U	0.4014	18.97

CHAPTER III

DATA ANALYSIS

A. Attenuation Cross Sections

The attenuation cross section measured by a counter having a solid angle $\Delta\Omega$ is given by the simple attenuation equation

$$\sigma_a(\Delta\Omega)=\frac{1}{nx}\ln(I_o/I_i) \tag{13}$$

where I_i is the intensity with the target in, I_o is the target out intensity, n is the density of nuclei in nuclei per cm^3, and x is the target thickness. The total cross section is obtained by extrapolating the attenuation cross section to zero solid angle. The standard approach is to simultaneously measure attenuation factors for a series of counters having different solid angles, then fit these data to some model. The zero solid angle attenuation cross section predicted by the best fit to the data is then taken to be the total cross section.

B. Corrections

Before the true attenuation cross section could be obtained several corrections had to be made on the raw data. The most significant correction required was the the rate effect discussed in Appendix II. This correction factor was determined by measuring the attenuation cross section for the Be target at a number of different rates and using the measured cross sections vs rate to obtain the relationship between the rate and the correction factor. The rate was

taken to be proportional to the target in and out average of the Delayed Cal(10%)·D1·$\overline{A}$ to Cal(10%)·D1·$\overline{A}$ ratio, hereafter called the "accidentals rate." Appendix III discusses the reasons for using this quantity as a measure of the rate. The σ_a (measured) vs accidentals rate data for the four transmission counters are shown in Fig. 8. The straight lines are least squares fits to the data using the linear expression

$$\sigma_a \text{ (measured)} = \sigma_a(1+aR) \qquad (14)$$

The average of the four values of a was taken as the correction factor for all elements and counters. Eq. (14) is derived in Appendix II. The best fit value of a was 0.031 $\pm$ 0.005. Most of the data required about a 2% rate correction.

A correction of the order of 1% was applied to the attenuation cross sections measured by the 7.75 in. counter, D1, in order to compensate for a gradual falloff in the calorimeter output amplitude towards the edge of the absorber plates. This correction was of little significance since D1 has little influence on the extrapolation to zero solid angle.

None of the targets were chemically analyzed specifically for this experiment; however, they were all obtained from the Lawrence Radiation Laboratory metal stores whose stock is specified by the Standards and Specification Group, Mechanical Engineering, Livermore Site, Lawrence Radiation Laboratory. According to these specifications the Cd, W and Pb targets were free of contaminants to the 0.1% level by weight. The

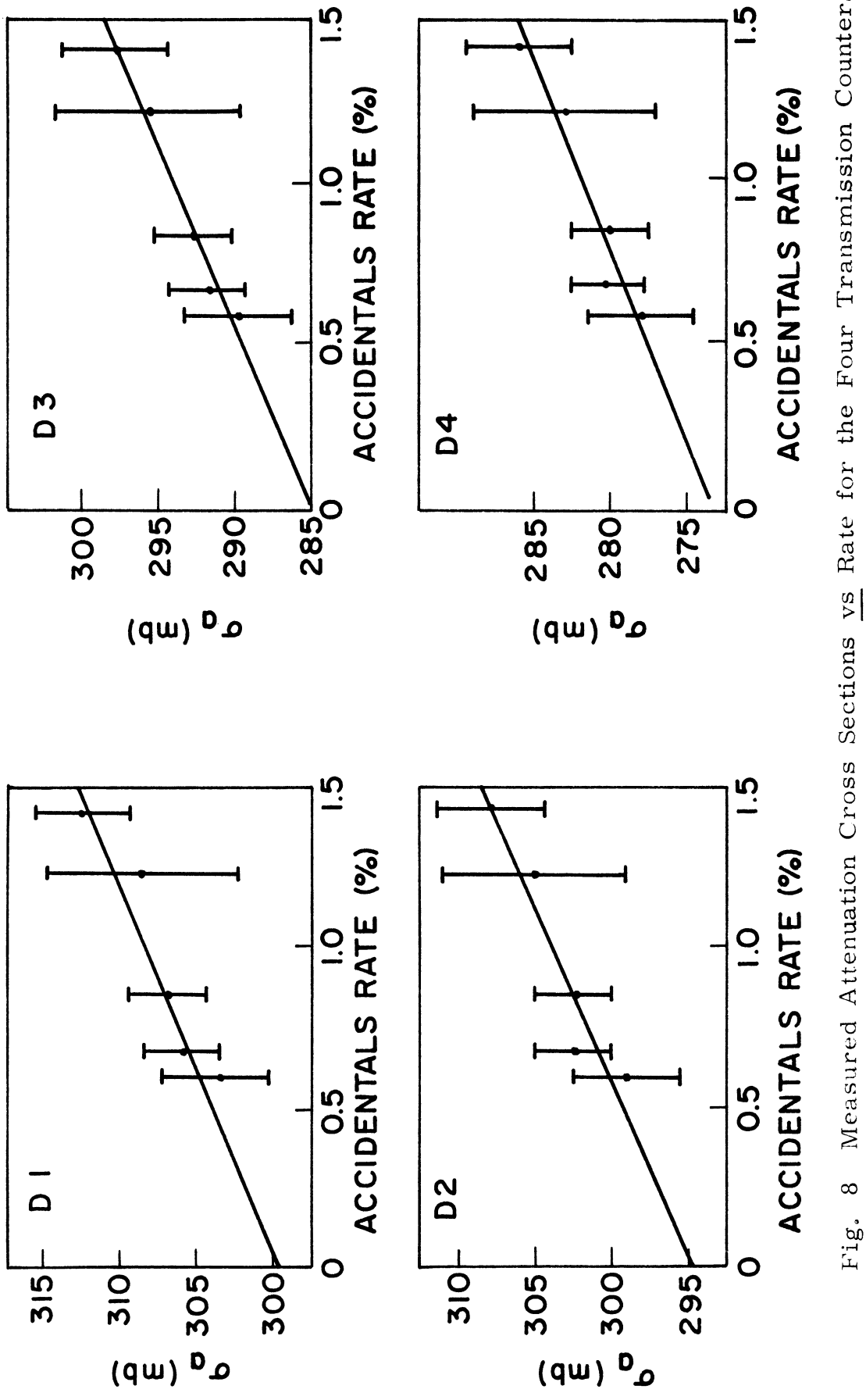

Fig. 8 Measured Attenuation Cross Sections vs Rate for the Four Transmission Counters

Be and Fe targets contained about 1% contamination, the most significant contaminants being Mn in the Fe and O in the Be. The closeness in A between the contaminants and the targets coupled with the weak A-dependence of the errors generated by the contaminants makes the error that results from ignoring them only of the order of 0.1% to 0.2%. This was not the case with aluminum as can be seen in Table IV, and a correction was required.

TABLE IV

Chemical Composition of Al Target

Element	% by Weight
Mg	$1.7\leq$, ≤ 2.3
Cu	$0.9\leq$, ≤ 1.5
Cr	$0.17\leq$, ≤ 0.4
Mn	≤ 0.3
Fe	≤ 0.7
Sn	≤ 0.6
Zn	$3.5\leq$, ≤ 4.2

Corrections were made for the various contaminants by dividing them into four groups according to atomic weight: those close to Al, Fe, Cu, and Cd in atomic weight. The target in readings for the four counters were then corrected for the additional attenuation produced by the contaminants.

A correction had to be made on the liquid target data to allow for the effects of the gas in the flask in the target

empty runs. This correction factor can be accurately determined if the temperature and composition of the gas is known; however, in this experiment the temperature was not measured. If we assume that the gas was totally helium, at 70 degrees K, in the hydrogen runs the correction would be 0.5%. If the gas were at 50 degrees K, the correction would be 0.8%, and 1.6% for 20 degrees K. Since a considerable quantity of room temperature helium was introduced to force the liquid out of the flask it seems reasonable not to expect the gas to be at the liquid temperature. Similarly one would not expect the gas to be above 70 to 80 degrees K, the temperature of the liquid nitrogen-cooled radiation shield. Therefore a temperature of 50 $\pm$ 20 degrees K was assumed. This corresponds to a correction factor of 0.8 $\pm$ 0.4% for the hydrogen and helium data. Since deuterium gas at 0.75 atmospheres was used in the deuterium runs the correction factor was 0.7 $\pm$ 0.4%.

C. Extrapolation to Zero Solid Angle

The corrected attenuation cross sections for the four counters are given in Table V. The uncertainties shown are the statistical errors of the raw data.

TABLE V

Corrected Attenuation Cross Sections
for the Four Transmission Counters

Element	Cross Sections (mb) D1	D2	D3	D4	Statistical uncertainty
H (6Gev/c)	42.56	42.17	41.43	38.91	0.74%
H (4Gev/c)	43.19	42.90	42.41	40.16	0.6 %
D (6Gev/c)	77.6	77.0	75.1	70.1	0.52%
D (4Gev/c)	80.1	79.3	78.3	73.8	0.6 %
Be	298.7	294.7	285.0	273.4	1.0 %
He	140.3	138.3	133.5	123.5	0.8 %
C	367.4	362.7	350.3	321.1	1.0 %
Al	710.4	695.1	649.0	478.1	1.35%
Fe	1229	1184	1071	931.0	1.35%
Cu	1371	1311	1181	1018	1.15%
Cd	2051	1941	1707	1453	1.0 %
W	2861	2672	2294	1964	0.9 %
Pb	3101	2888	2470	2107	0.8 %
U	3456	3182	2706	2311	1.05%

Three extrapolation methods were tried. The first assumed that the measured attenuation cross sections decrease linearly with solid angle so that the total cross section is given by

$$\sigma_t=\sigma_a(i)+ [\sigma_a(i)-\sigma_a(i+1)]\cdot\Delta\Omega(i)[\Delta\Omega(i+1)-\Delta\Omega(i)]^{-1} \quad (15)$$

where $\sigma_a(i)$ is the attenuation cross section measured by the ith counter, $\Delta\Omega(i)$ is the solid angle of the ith counter with $\Delta\Omega(i)<\Delta\Omega(i+1)$. This is only valid if $d\sigma/d\Omega$ is constant over

the solid angles subtended by the counters. Therefore it is only applicable to the smallest counters for the high A targets but is good for all four counters for the low A targets.

The second method assumed that the difference between the attenuation cross section and the total cross section is due to small angle elastic scattering and that $d\sigma/d\Omega$ is represented by the expression for scattering from a totally absorbing disc, i.e.

$$\sigma_t = \sigma_a(i) + \left[\frac{k\sigma_t}{4\pi}\right]^2 \int \left\{\frac{2J_1(Rk\theta)}{Rk\theta}\right\}^2 f_i(\theta)\, d\Omega \qquad (16)$$

where $f_i(\theta)$ is the geometrical response function of the ith transmission counter (see Appendix), and R is the nuclear radius. Actually allowance should be made for the fact that the neutron beam was not monoenergetic. However that refinement represents a neglilible improvement in this case. Total cross section values were calculated using Eq. (16) for all four values of $\sigma_a(i)$, treating R as a free parameter. Very good agreement could be obtained between the four values of σ_t for reasonable R values for all of the heavy targets. The σ_t values calculated from the larger counters for the lighter elements, however, were slightly smaller than the smaller counter values. This is to be expected since no inelastic term is included in Eq. (16). This was not noticeable for the heavy targets since the elastic correction is so large. However for the lighter elements where the elastic correction is small, the inelastic term is not compeletely negligible for the largest counter.

The third approach was to make a least squares fit to a polynomial in $|t|$, i.e.

$$\sigma_a(i)=\sigma_t+a|t|+b|t|^2+c|t|^3. \qquad (17)$$

The total cross section values yielded by these three extrapolation methods were averaged to obtain the final cross sections, and the spread among the methods was taken as a measure of the uncertainty. In all cases this spread was small compared to the statistical uncertainty of the data. Table VI shows the cross sections obtained from these three methods for several elements.

TABLE VI

Cross Sections Obtained from the Three Extrapolation Techniques

Element	Extrapolation Method			Percentage spread
	#1	#2	#3	
H	42.57	42.40	42.40	± 0.2
D	77.92	77.73	77.90	± 0.13
Cu	1410	1400	1410	± 0.35
Cd	2114	2112	2121	± 0.2
U	3608	3618	3634	± 0.35

CHAPTER IV

RESULTS

A. Measured Total Cross Sections

The total cross sections resulting from the analysis procedures discussed in Chapter III are listed in Table VII. The uncertainties represent the uncertainties associated with the various correction factors discussed in Chapter III and the statistical uncertainty of the experimental data combined in quadrature.

TABLE VII

Total Cross Sections

Element	Z	A	Total cross section (mb)	
			5.7 Gev/c	4.0 Gev/c
H	1	1	42.5±0.6	43.1±0.6
D	1	2	77.8±1.3	80.3±1.9
He	2	4	142±3	
Be	4	9	301±5	
C	6	12	370±6	
Al	13	27	718±13	
Fe	26	56	1250±20	
Cu	29	64	1410±30	
Cd	48	112	2120±30	
W	74	184	2970±70	
Pb	82	207	3240±50	
U	92	238	3620±60	

B. Comparison With Other np and nd Data

Figs. 9 and 10 show the available np and nd total cross sections above 1 Gev/c. The Bugg et al.[3], Foley et al.[2], and Galbraith et al.[5] pp data are shown in Fig. 11. As can be seen, the np values from this experiment are somewhat higher than the Engler et al.[13] results. However since their experiment did not contain a neutron energy selecting element, this discrepency may be due to the fact that their values are averages over an energy range where the cross section is changing fairly rapidly. Their nd data also appears low relative to the pd data. The 5.7 Gev/c nd value of this experiment is in good agreement with the Galbraith et al.[5] 6 Gev/c pd cross section, and our 4.0 Gev/c nd value is consistent with the Bugg et al.[3] 4.0 Gev/c pd value.

It is interesting to compare the energy dependence of the np cross section (Fig. 9) with the pp cross section (Fig. 11). The nucleon-nucleon, antinucleon-nucleon, and $K^{\pm}$-nucleon total cross sections can be expressed in terms of the cross sections for pure isospin states, I = 0 and I = 1. The pp, $\bar{p}n$, K^-n, and K^+p cross sections are pure I = 1 cross sections and the np, K^-p, $\bar{p}p$, and K^+n cross sections are made up of equal parts of I = 0 and I = 1 cross sections. Experimentally it is found that, in the case of K-nucleon and antinucleon-nucleon cross sections, the I = 0 cross section is equal to or larger than the I = 1 cross section.[5] If the same is true for the nucleon-nucleon interactions the np cross section

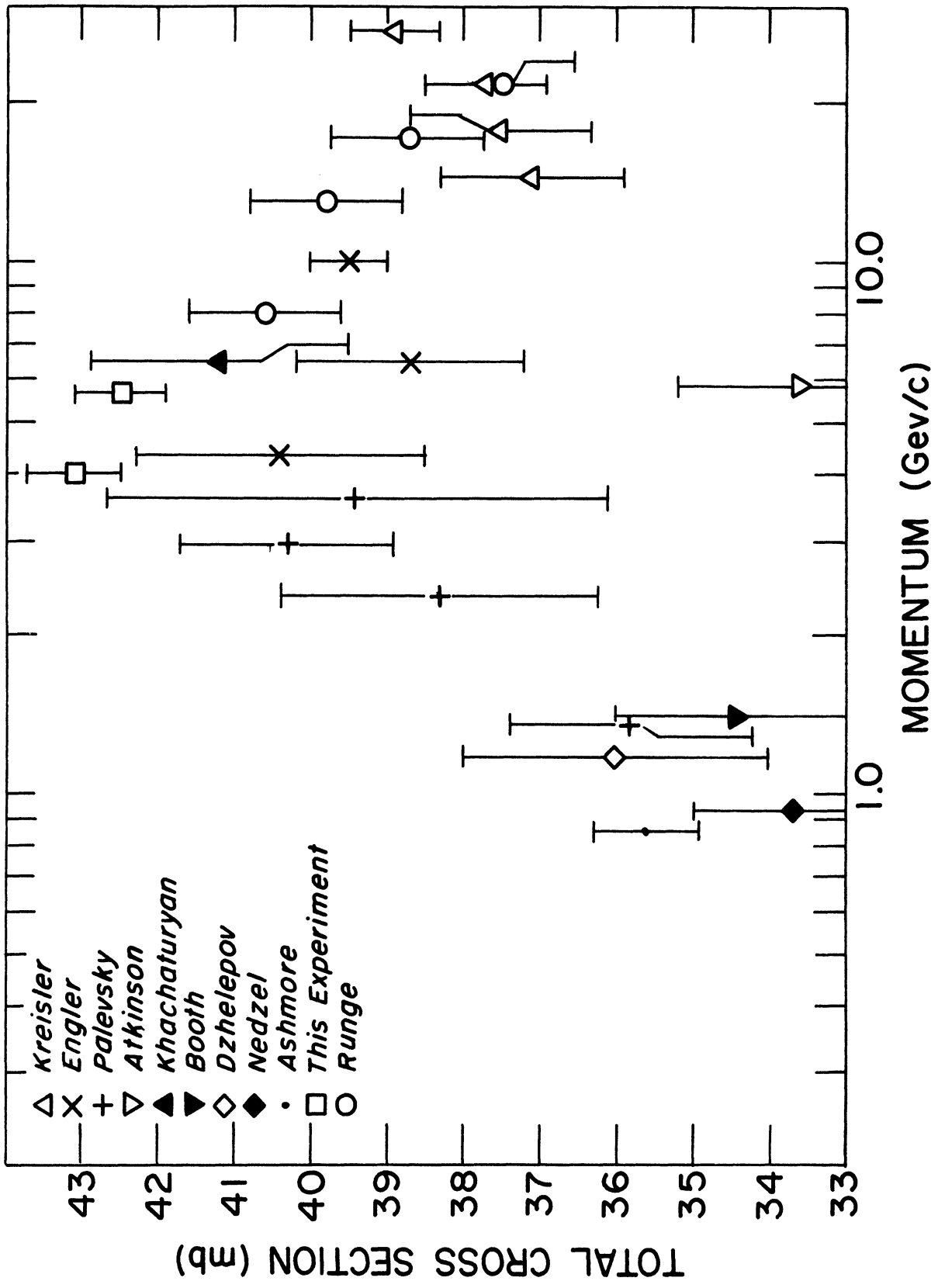

Fig. 9 Neutron-Proton Total Cross Section

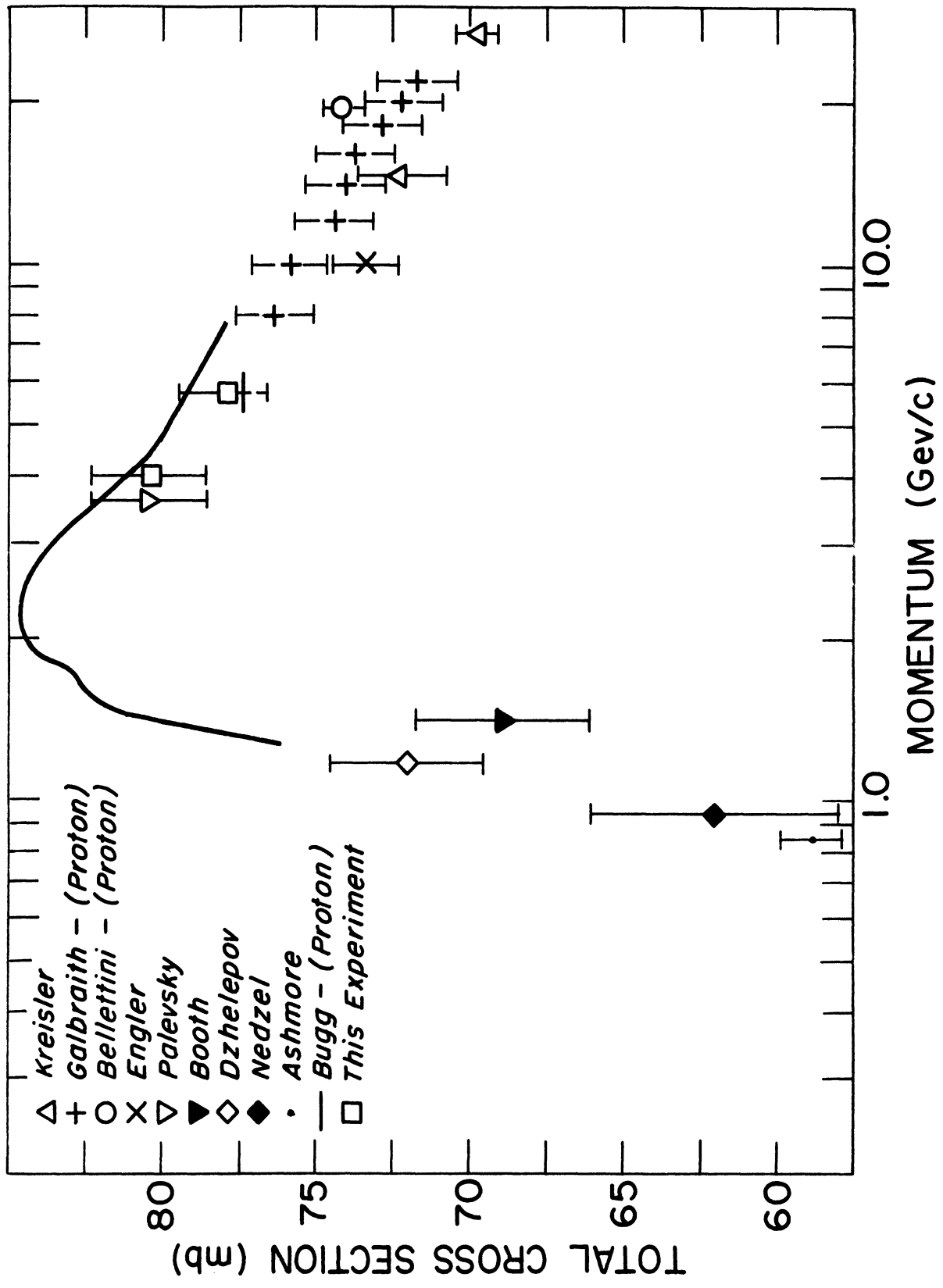

Fig. 10 Deuterium Total Cross Section

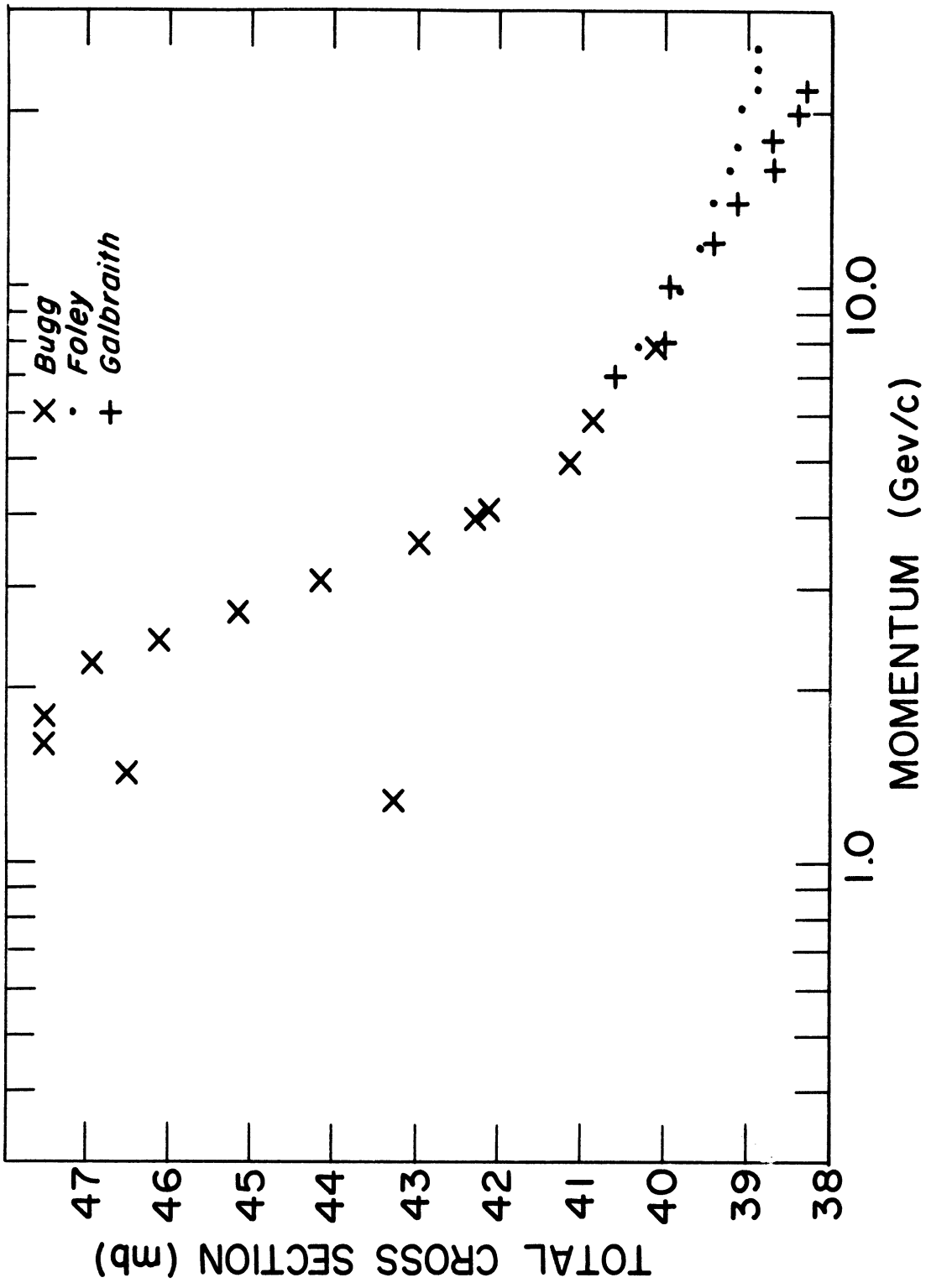

Fig. 11 Proton-Proton Total Cross Sections

should be equal to or greater than the pp cross section. A comparison of Figs. 9 and 11, however, shows that $\sigma(np)$ seems to oscillate around $\sigma(pp)$ with $\sigma(np)$ less than $\sigma(pp)$ below 3.5 Gev/c and again from about 12 to 27 Gev/c. It must be noted, however, that only the 22 Gev/c np point is definitely below the pp curve and without it there would be little evidence for a crossover.

C. Deuteron Screening Correction

One can use Eq. (1) through (4) and the assumption of charge independence to calculate values for the deuteron screening correction factor,

$$\delta=[\sigma(pp)+\sigma(np)-\sigma(nd)]/[\sigma(pp)+\sigma(np)]$$

and the quantity

$$\langle r^{-2}\rangle(1-\alpha_{np}\alpha_{pp})=4\pi[\sigma(pp)+\sigma(np)-\sigma(nd)]/\sigma(pp)\sigma(np)$$

from the cross sections listed in Table VII. The results are shown in Table VIII. Also included are values obtained using the preliminary np data of Runge[39] et al. Figs. 12 and 13 show the values of these quantities obtained from the earlier experiments. The theoretical values shown in these figures are those calculated by Bugg et al.[3] for a Hulthén wave function and a value of 9.6 for b in Eq. (8). The earlier data exhibit a strong energy dependence contrary to the theoretical predictions of Glauber[27] or Pumplin and Ross.[30] If the values obtained with the Bugg et al.[3] pd data are omitted the remainder of the nucleon data are consistent with

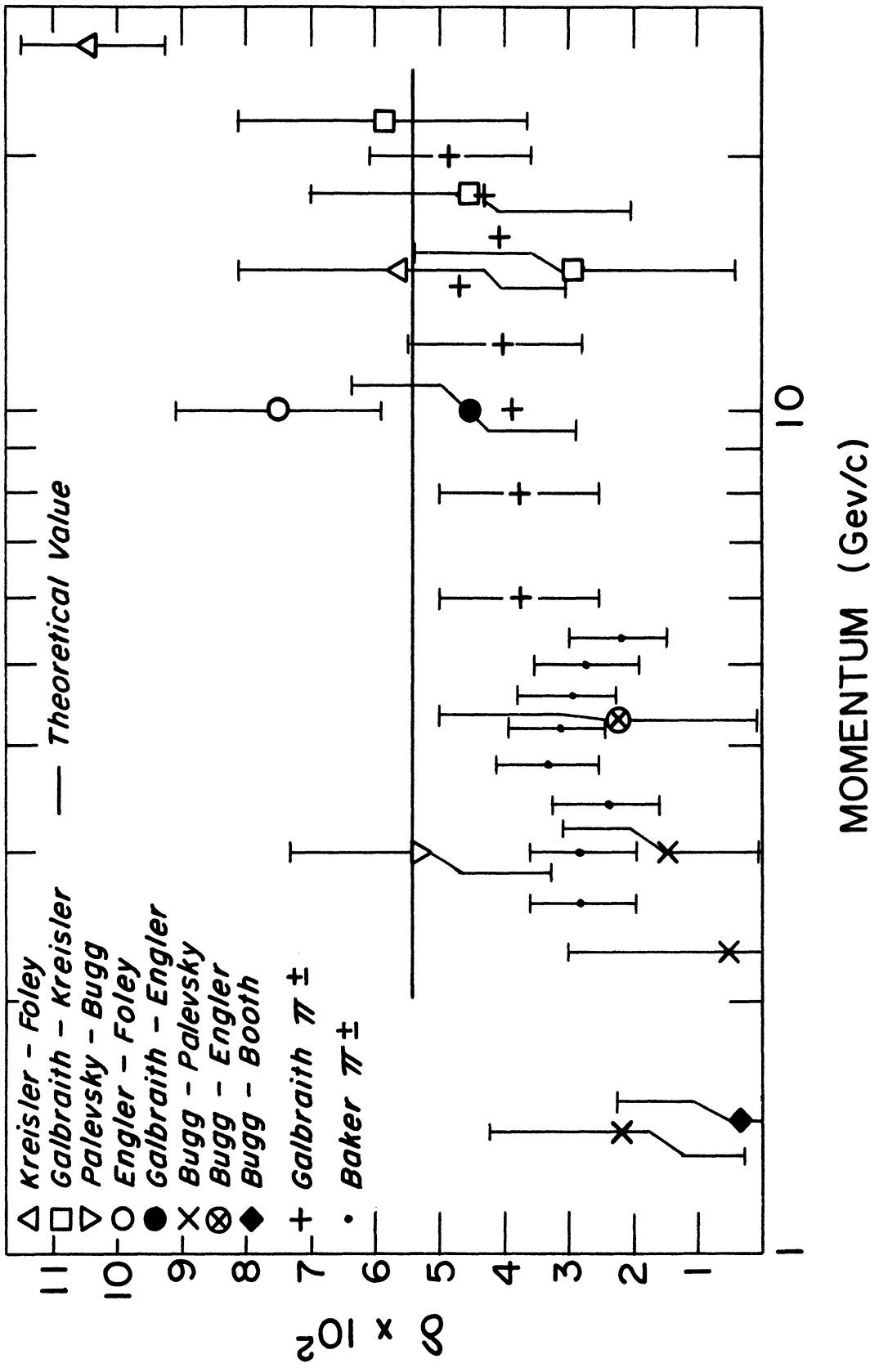

Fig. 12 Deuteron Screening Factor

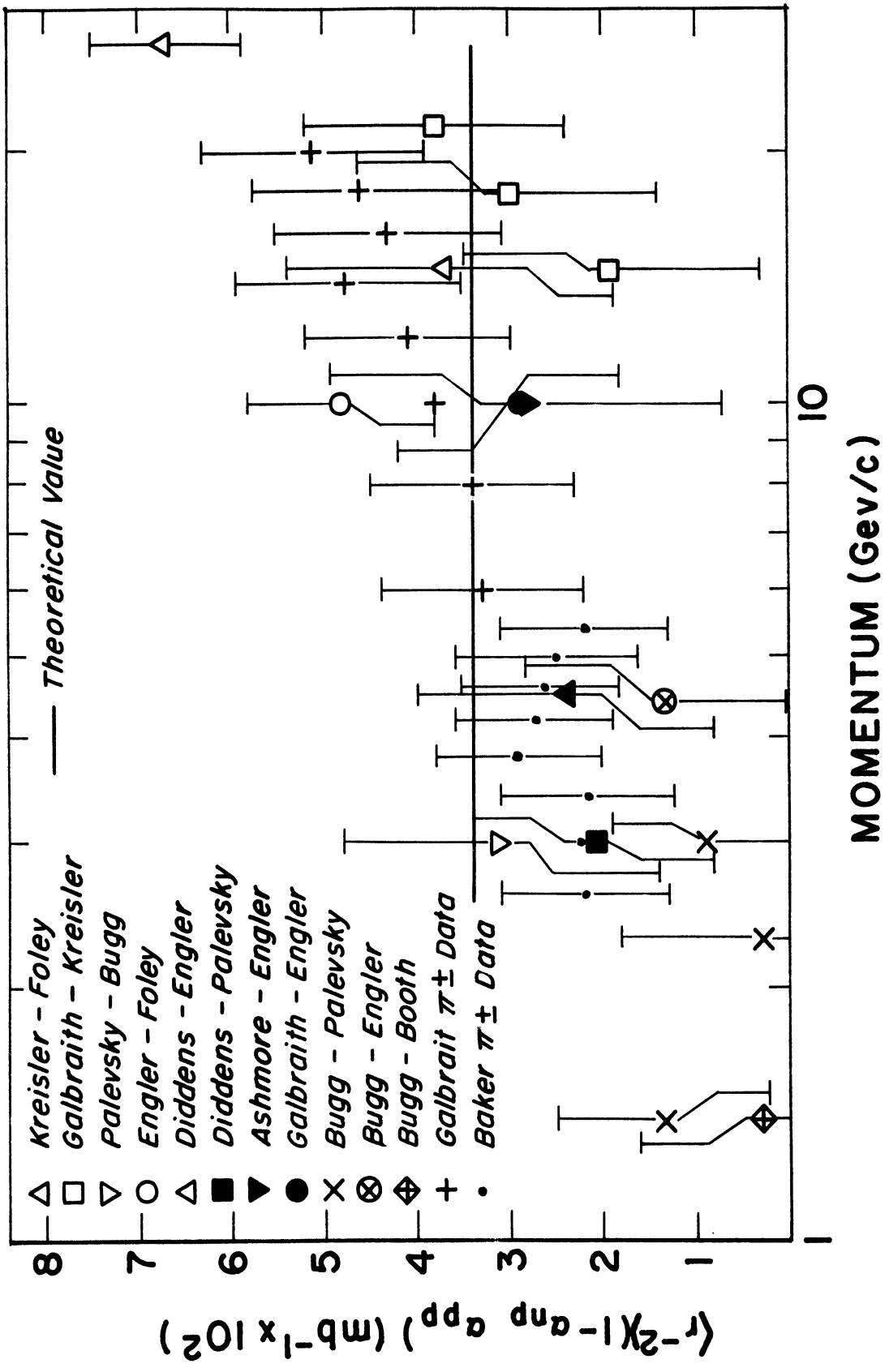

Fig. 13 Glauber Screening Term

TABLE VIII

Deuteron Screening Term

P (Gev/c)	$\sigma_t(pp)$ (mb)	$\sigma_t(np)$ (mb)	$\sigma_t(pd)$ (mb)	$\sigma_t(nd)$ (mb)	$\langle r^{-2} \rangle (1-\alpha_{np}\alpha_{pp})$ $\times 10^2 mb^{-1}$	$\delta \times 10^2$
6	40.6^{5} ± 0.6	42.5^{x} ± 0.6	77.4^{5} ± 1.3		4.1 ± 1.1	6.8 ± 1.6
6	"	"		77.8^{x} ± 1.3	3.8 ± 1.1	6.4 ± 1.6
6	40.8^{3} $\pm .12$	"	79.1^{3} $\pm .25$		3.0 ± 0.5	5.0 ± 0.7
6	"	"		77.8^{x} ± 1.3	4.0 ± 1.0	6.6 ± 1.4
4	42.1^{3} $\pm .12$	43.1^{x} ± 0.6	80.9^{3} $\pm .25$		3.0 ± 0.5	5.0 ± 0.7
4	"	"		80.3^{x} ± 1.9	3.4 ± 1.4	5.7 ± 1.9
8	40.0^{5} ± 0.6	40.6^{39} ± 1.0	76.2^{5} ± 1.3		3.4 ± 1.3	5.5 ± 1.7
13	39.2^{5} ± 0.6	39.8^{39} ± 1.0	74.2^{5} ± 1.3		3.8 ± 1.3	6.1 ± 1.7
17	38.7^{5} ± 0.6	38.7^{39} ± 1.0	73.2^{5} ± 1.3		3.5 ± 1.4	5.8 ± 1.7
22	38.3^{5} ± 0.6	37.5^{39} ± 1.0	71.6^{5} ± 1.3		3.7 ± 1.4	5.5 ± 1.7
theoretical value					3.4	5.4

x this experiment

a constant or weakly energy dependent screening factor except for the 27 Gev/c point of Kreisler et al.[14] The agreement among the values in Table VIII is quite good and is consistent with a constant or nearly constant screening factor. The agreement with the theoretical values is also quite good.

D. Charge Independence

The nn total cross section can be evaluated from Eq. (4) using the Galbraith et al.[5] experimental value for the Glauber screening term, i.e. 0.042 ± 0.003 mb^{-1}. From charge symmetry it is expected to equal the pp cross section. We also expect $\sigma(pd)=\sigma(nd)$ from charge symmetry. Table IX compares these cross sections. The agreement is good.

TABLE IX

Comparison of $\sigma(nn)$, $\sigma(pp)$ and $\sigma(nd)$, $\sigma(pd)$ at 4 and 6 Gev/c

Momentum (Gev/c)	$\sigma(pp)$ (mb)	$\sigma(nn)$ (mb)	$\sigma(pd)$ (mb)	$\sigma(nd)$ (mb)
4	$42.1\pm.12$[3]	43.5 ± 2.4[x]	$80.9\pm.24$[3]	80.3 ± 1.9[x]
6	$40.6\pm.6$[5]	41.2 ± 1.7[x]	77.4 ± 1.3[5]	77.8 ± 1.3[x]
6	$40.8\pm.12$[3]		$79.1\pm.24$[3]	

x this experiment

E. Nuclear Total Cross Sections

Sievers[40] has derived a rather simple expression for fitting nuclear total cross section data in terms of two parameters, the nucleon radius, a_o, and the nucleon mean free path in nuclear matter, x_o. The expression is

$$\sigma = 2\pi\left\{R^2 - 2\left[1-(\lambda R+1)e^{-\lambda R}\right]/\lambda^2\right\} \qquad (18)$$

where $R=a_o A^{1/3}$, A is the atomic weight, and $\lambda=2/x_o$. This is obtained in an optical model, by integrating, for zero degree scattering, the familiar small angle, large ℓ_{max} integral approximation for the scattering amplitude,[41] i.e.

$$f(\theta)=ik\int_0^\infty b\ a(b)\ J_o(kb\theta)db, \tag{19}$$

assuming a totally absorptive interaction. With this assumption the partial wave amplitude, a(b), (where b is the impact parameter) becomes the absorption probability which should depend upon the amount of nuclear matter traversed by the particle, i.e.

$$a=(1-e^{-x/x_o}), \tag{20}$$

where x is the total path length of the particle in the absorbing medium. If we now assume that the direction of the incident particle is unchanged in traversing the nucleus Eq. (20) becomes

$$a(b)=(1-e^{\frac{-2\sqrt{R^2-b^2}}{x_o}}) \tag{21}$$

Combining Eq. (19) and (21) and integrating we get Eq. (18).

Eq. (18) was fitted to the total cross sections listed in Table VII using a trial and error least squares method. The best fit is shown in Fig. 14 along with the experimental points. The best fit parameters are $a_o=1.27\pm0.01$f, which is in good agreement with the values of 1.2f to 1.3f obtained from electron scattering, and $x_o=3.0\pm0.2$f. The optical thickness vs impact parameter for six elements is shown in Fig. 15.

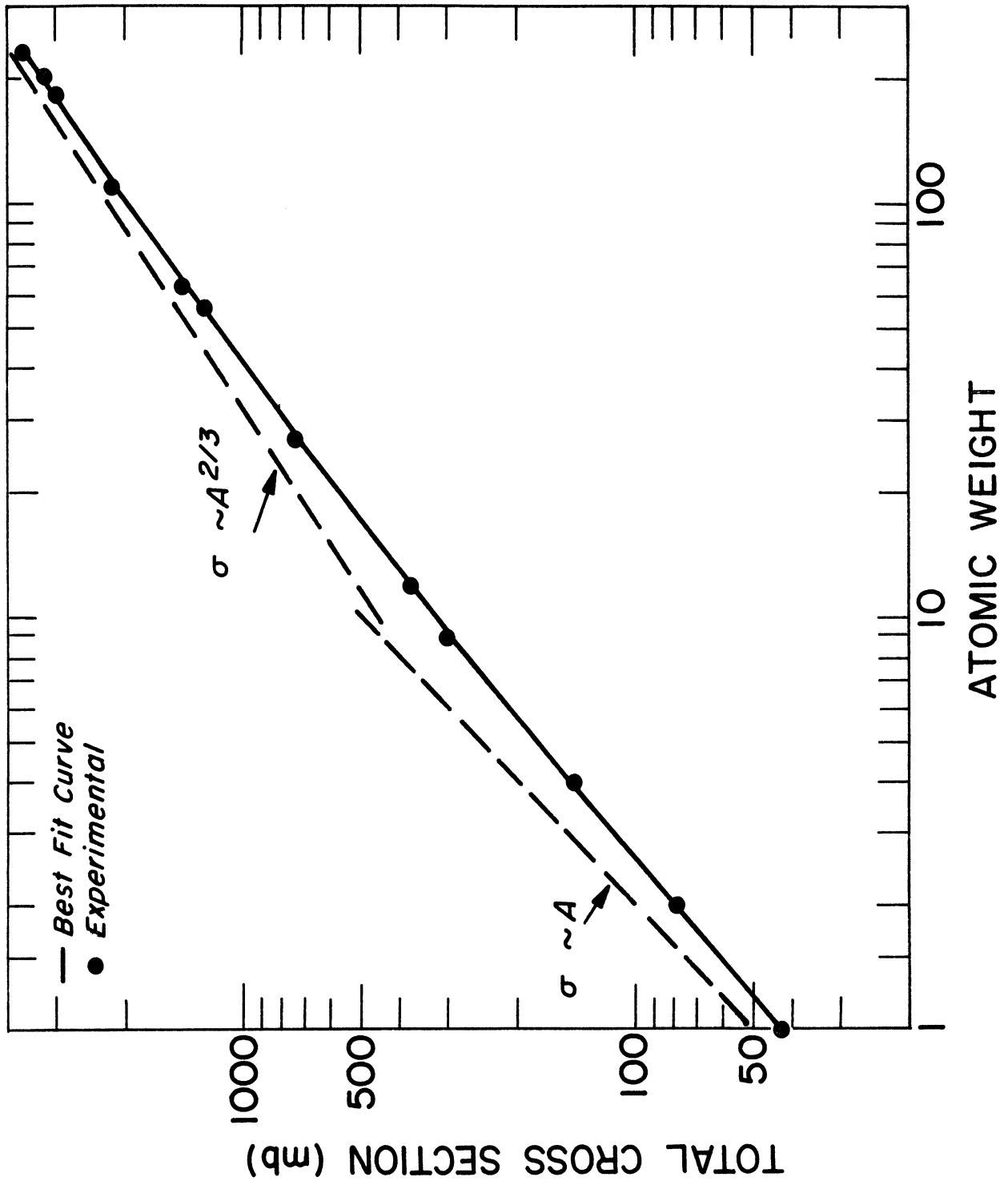

Fig. 14 Best σ vs A Absorption Model Fit

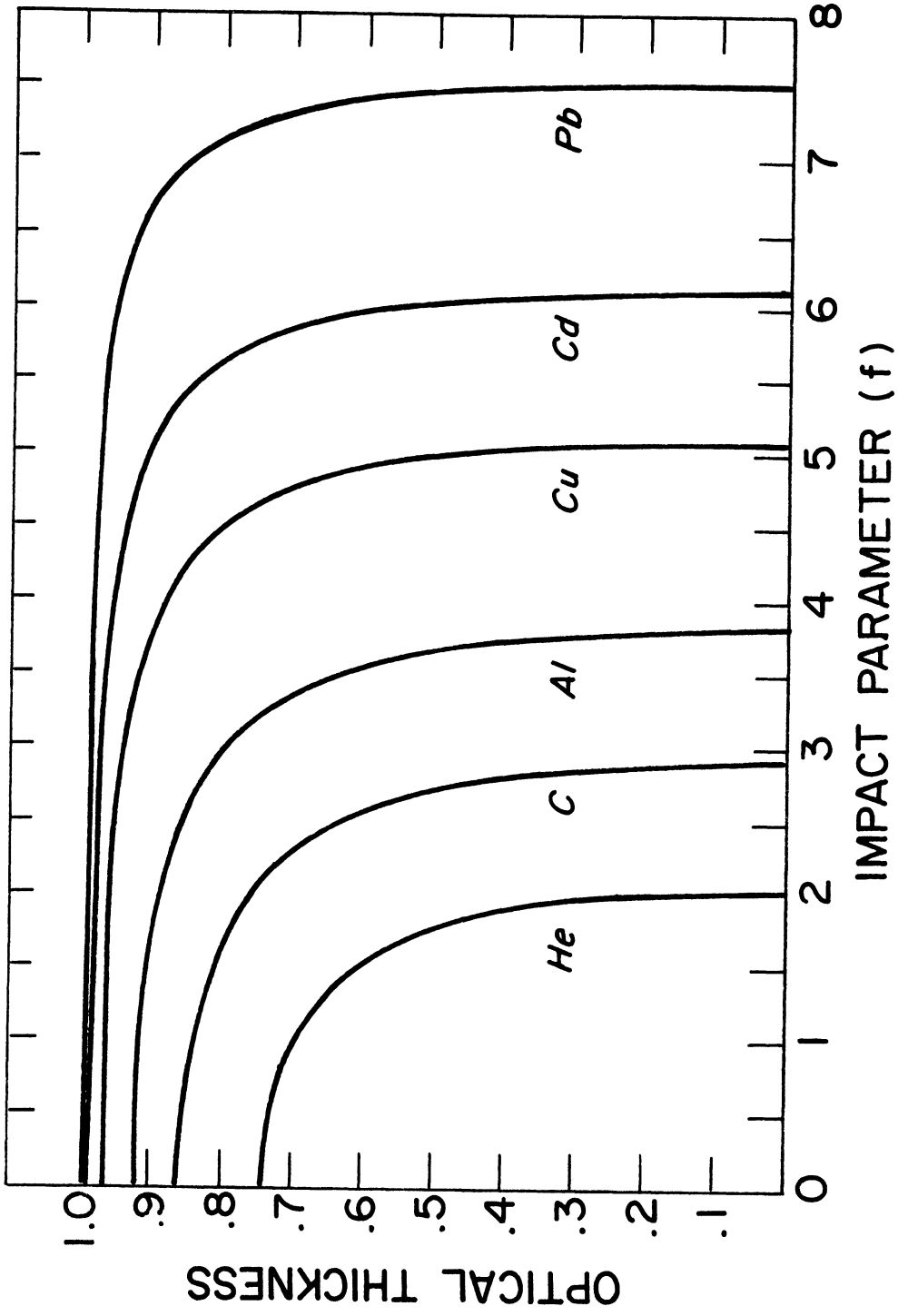

Fig. 15 Optical Thickness for He, C, A1, Cu, Cd and Pb

As can be seen, He is quite transparent while Pb is almost totally opaque. The nuclear radii obtained from this value of a_o, i.e. $R=a_o A^{1/3}$, are in quite good agreement with the radii which yielded the best agreement between the four values of σ_t obtained when using Eq. (16) to extrapolate the attenuation cross sections to zero solid angle in Chapter III.

F. Comparison With Other Nucleon-Nuclear Data and the Energy Dependence of the Total Cross Sections

In order to show how the results of this experiment compare with previous experiments the available nucleon-nuclear total cross section data were collected and are presented in Figs. 17 through 21 for those elements for which considerable data exist. Also included are the preliminary results from a recently completed CERN neutron experiment[39] that included an ionization calorimeter for energy selection. The dashed lines are included in the figures only to guide the eye. The only previous measurement at about 6 Gev/c is that of Atkinson *et al.* which seems to be incorrect. The agreement between this experiment and the preliminary results from CERN is very good.

Fig. 21 is a plot of the nuclear screening correction factor, δ, for several elements calculated using Eq. (11) and the pp, np, and n-nuclear data presented in this chapter. The calculated values of Pumplin and Ross[30] are included. The data are consistent with a constant δ, especially in the case of lead and aluminum. However, it must be noted that the

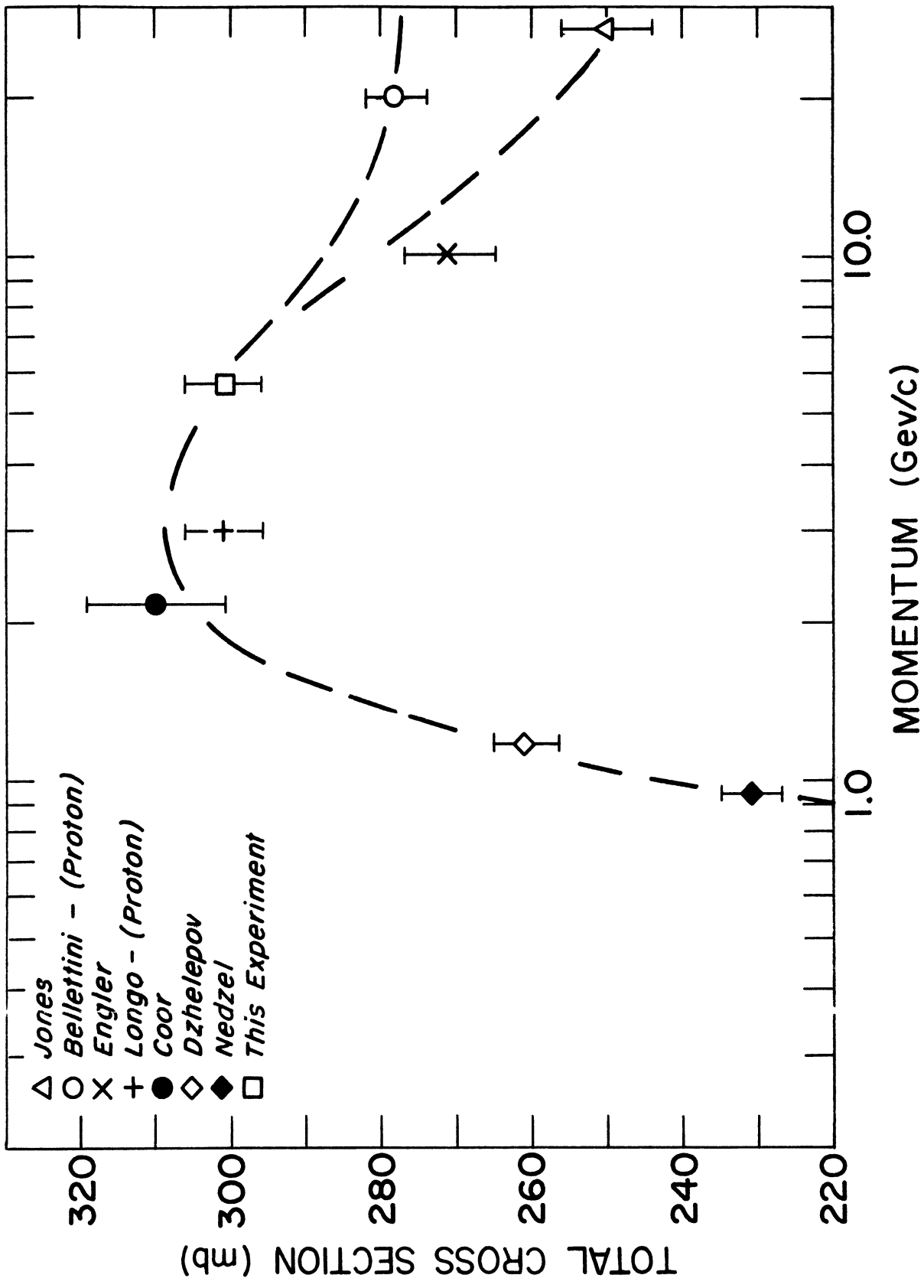

Fig. 16 Beryllium Total Cross Section

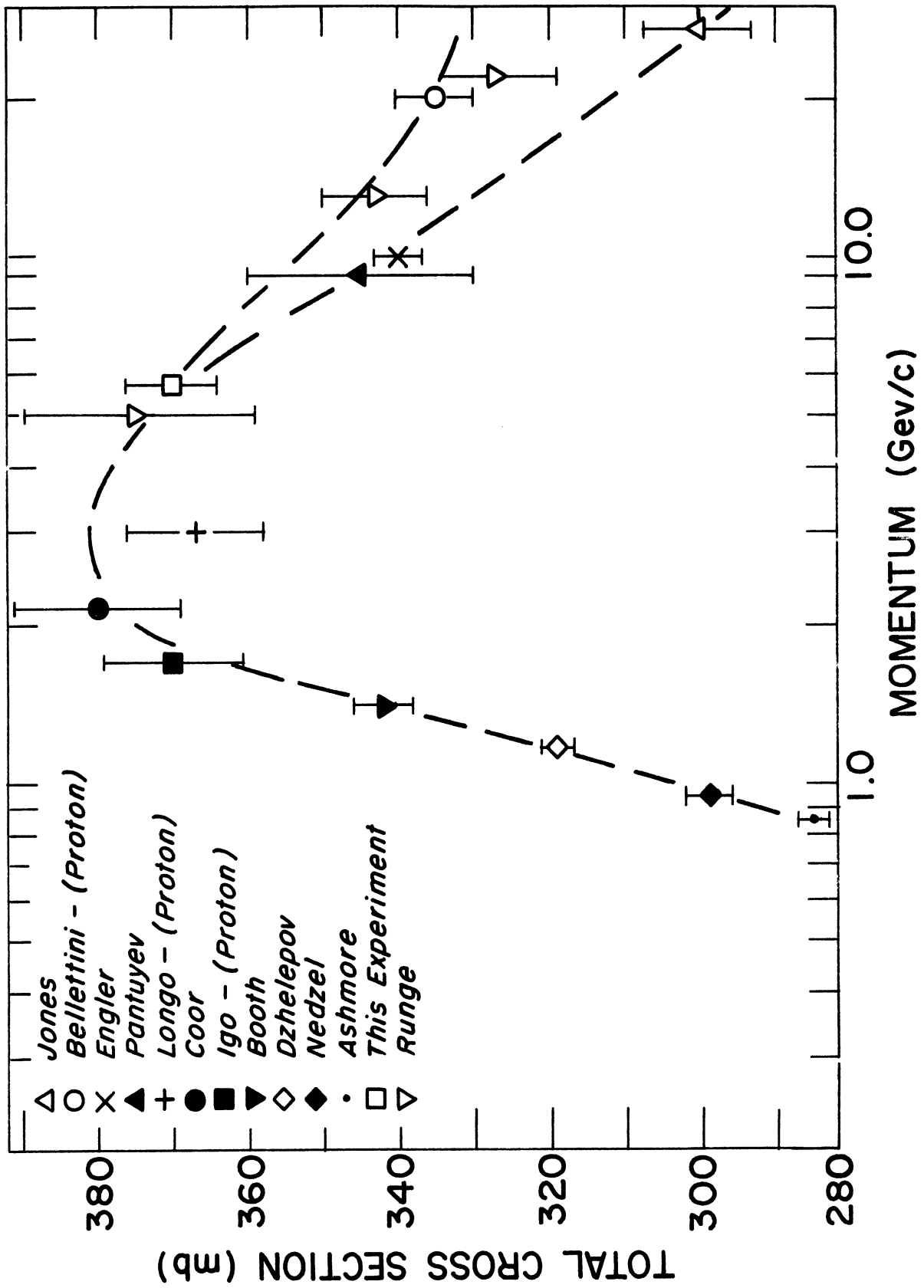

Fig. 17 Carbon Total Cross Section

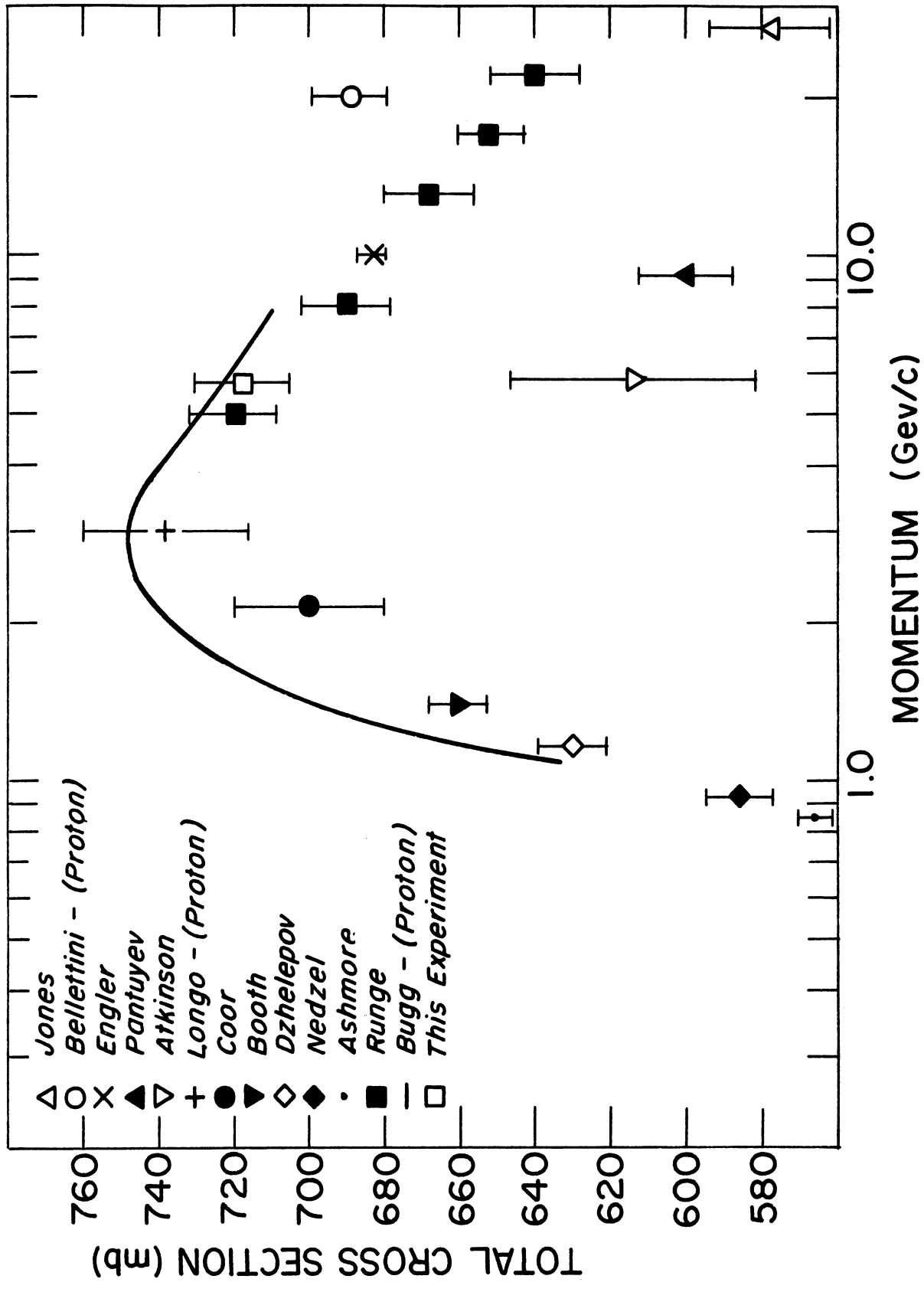

Fig. 18 Aluminum Total Cross Section

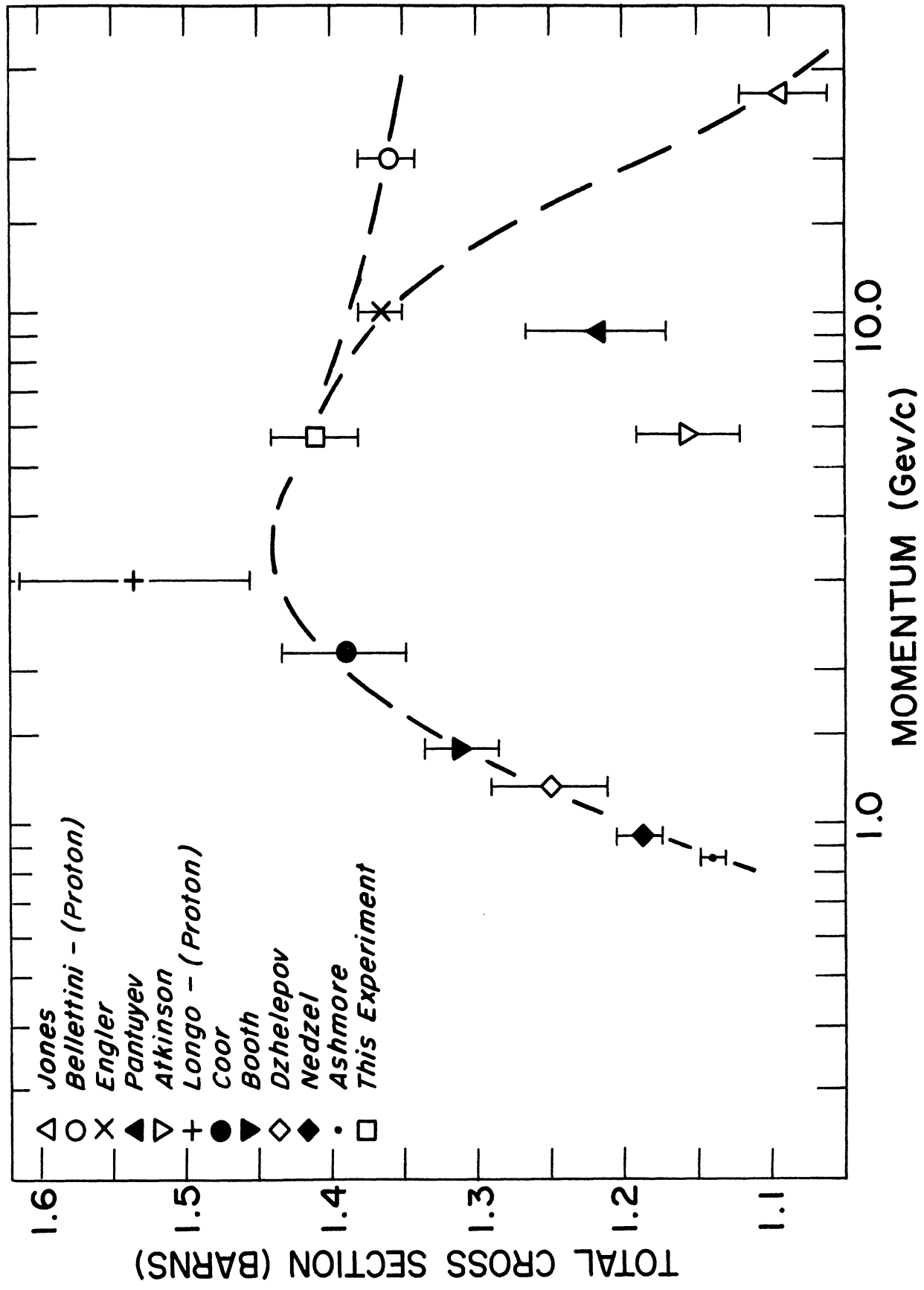

Fig. 19 Copper Total Cross Section

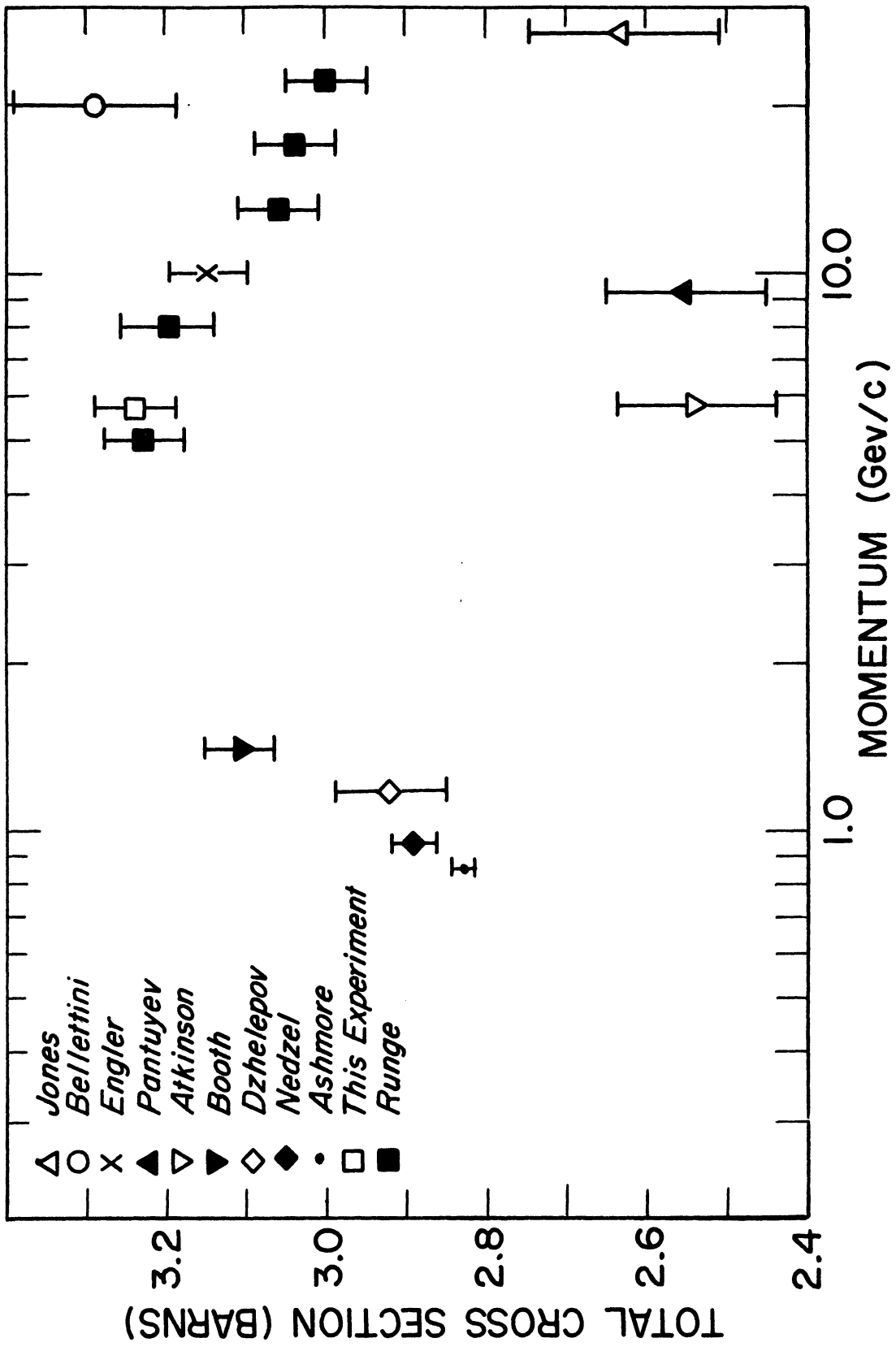

Fig. 20 Lead Total Cross Section

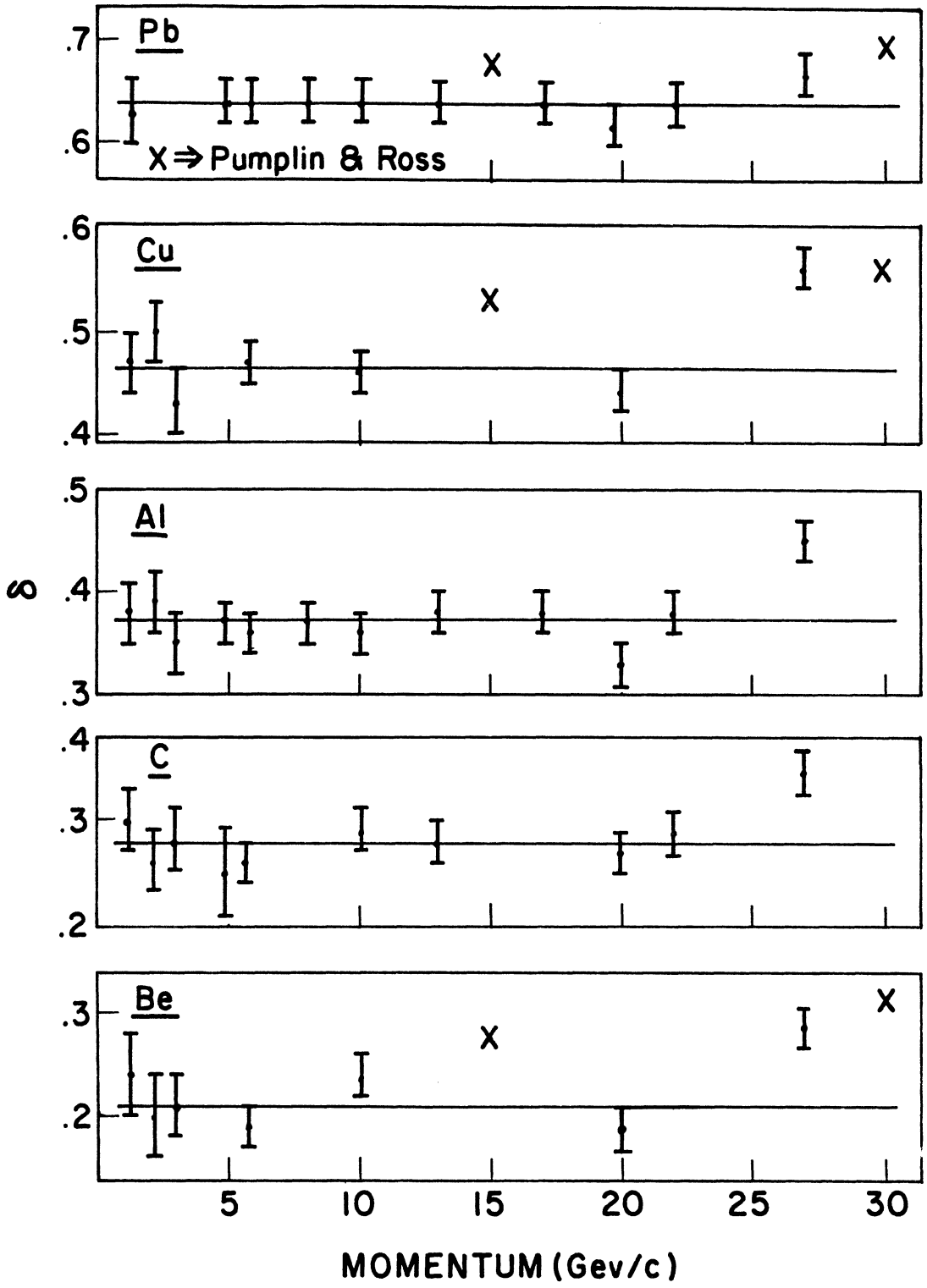

Fig. 21 δ vs Momentum for Be, C, A1, Cu, & Pb.

key points between 10 and 22 Gev/c are based on preliminary data. The data are not inconsistent with the Pumplin and Ross model.

Except for the 27 Gev/c point the average values of δ for the data shown in Fig. 2 fit an $A^{0.26}$ expression quite well for $A \geq 12$. This suggest the following empirical equation for relating nucleus cross sections to the nucleon-nucleon cross section;

$$\sigma(nA)=[(A-Z)\sigma(pp)+ Z\sigma(np)][1-0.155A^{.26}] \quad (22)$$

$$\sigma(pA)=[(A-Z)\sigma(np)+ Z\sigma(pp)][1-0.155A^{.26}] \quad (23)$$

CHAPTER V

CONCLUSION

The neutron-proton and neutron-deuteron total cross sections have been measured to an accuracy of 1.5% at 4.0 and 5.7 Gev/c. These cross sections, along with those obtained by Runge *et al.*[37] show that $\sigma(np) \geq \sigma(pp)$ below 10-15 Gev/c. The experimental data between 10-15 Gev/c and 27 Gev/c indicate $\sigma(np) \leq \sigma(pp)$, which is contrary to the available data on the relative sizes of the pure I=0 and I=1 amplitudes. The region above 15 Gev/c should be investigated further to determine if this is indeed true and whether or not $\sigma(np) \geq \sigma(pp)$ above 27 Gev/c.

The deuteron screening factor was evaluated and was found to be consistent with the theoretical predictions. The experimental uncertainties are, however, too large to prove or disprove the existence of an inelastic contribution of the size predicted by Pumplin and Ross.[30]

The neutron-nuclear total cross sections were measured for He, Be, C, Al, Fe, Cu, Cd, W, Pb, and U at 5.7 Gev/c. These data fit a totally-absorbing optical model quite well. All of the available high-energy nucleon-nuclear total cross section data were used to evaluate the nuclear screening factor as a function of momentum for several elements. These data are consistent with a momentum independent screening factor; however, the uncertainties are too large to disprove the existence of a momentum dependence of the size predicted

by Pumplin and Ross.[30] A reevaluation of the 27 Gev/c cross section should clarify this question.

APPENDIX I

CALORIMETER RESPONSE

Since a high-energy monoenergetic neutron beam is not technically feasible the energy resolution of the calorimeter could only be determined indirectly. This determination was made by trying to find an energy resolution function that, coupled to the incident neutron spectrum, would produce a good fit to the measured calorimeter attenuation or integral pulse height distribution curves (see Fig. A-1). It was assumed that the incident neutron spectrum was given by Eq. (12) up to 0.3 Gev/c of P_b and then fell linearly to zero at P_b (see Figs. A-2 and A-3). It was also assumed that the energy resolution of the calorimeter was energy independent, i.e. a monoenergetic neutron beam would give a Gaussian pulse height spectrum with a FWHM, ΔE, equal to some constant, C, times the neutron energy, E. Fig. A-1 shows attenuation curves taken at two Bevatron energies along with the fit obtained for C=1.5. This indicates that the calorimeter resolution was $\pm$ 75%.

The output of the calorimeter was fanned out to two discriminators, one set to trigger only on the largest 10% of the calorimeter output pulses, the other set to trigger on the largest 50%. The effective neutron spectra for these two discriminator settings for Bevatron energies of 3.7 and 5.4 Gev are shown in Figs. A-2 and A-3.

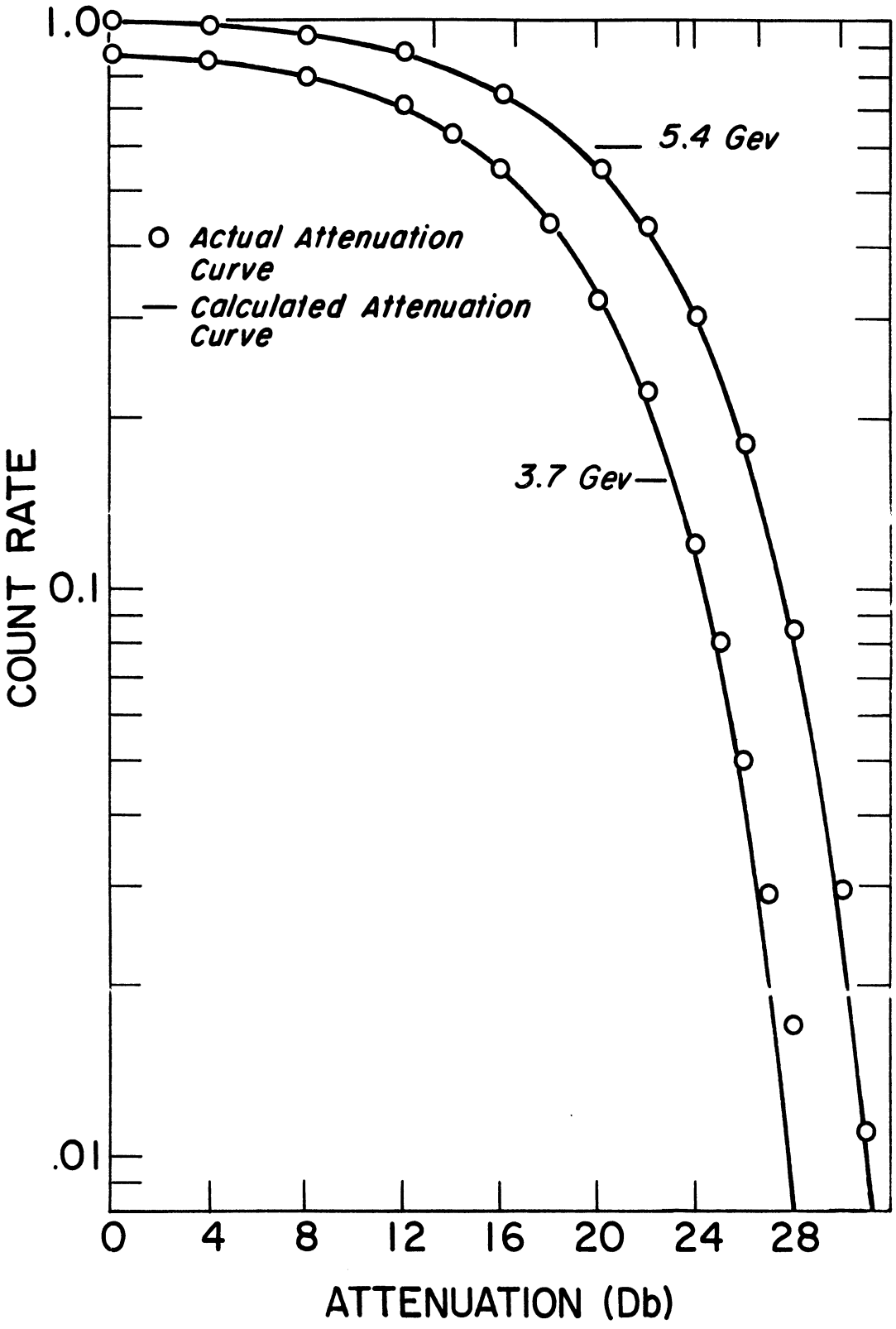

Fig. A-1 Actual and Calculated Attenuation Curves for a 3.7 and 5.4 Gev Peak Energy Neutron Beam

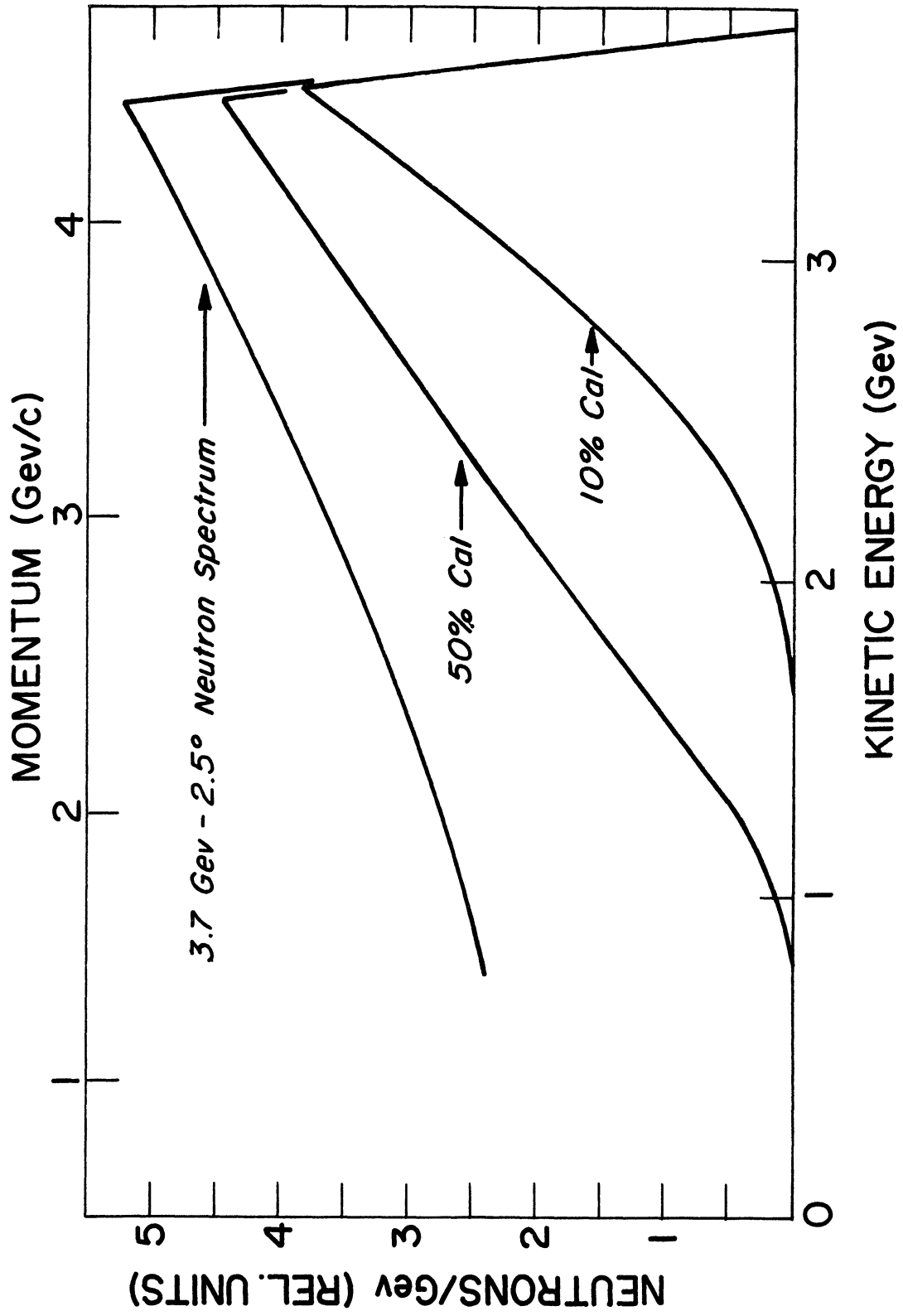

Fig. A-2 Incident and Effective Neutron Spectra for a 3.7 Gev Beam Energy

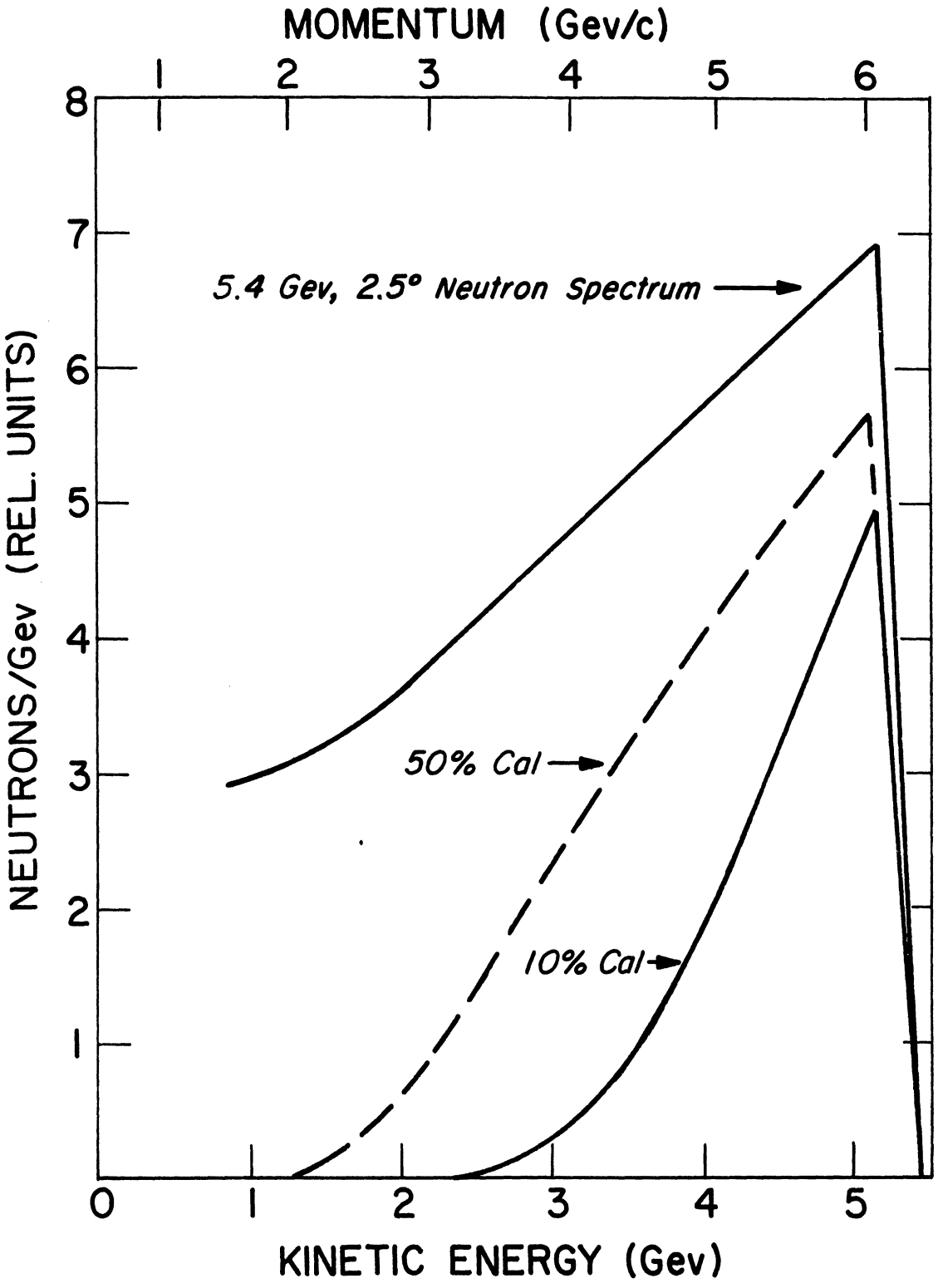

Fig. A-3 Incident and Effective Neutron Spectra for a 5.7 Gev Beam Energy

APPENDIX II

RATE EFFECT

A. Signal to Noise Ratio

With the 0.5 in. thick iron converter plate there was about a 10% probability that an incident neutron would undergo a conversion in the iron while there was about an 80% probability for a neutron to convert in the body of the calorimeter. Since the calorimeter discriminator rejected all but the upper 10% of the pulses from neutron conversions occuring in the iron plate, the ratio of the "signal" pulses to the "noise" pulses coming from the calorimeter was of the order of 0.01.

A small ratio like this would not be a problem at the average beam intensities used in this experiment; however, because of RF structure and strong magnet ripple modulation, the beam contained spikes with intensities many times larger than the average. During these spikes the probability that the pulses from two uncorrelated neutron interactions add to produce a pulse large enough to trigger the calorimeter discriminator becomes significant. A discussion on the effect of these pile-up pulses on the cross section measurements is given below.

B. Rate Effect on Measured Total Cross Sections

The probability that the pulses from two uncorrelated neutron interactions in the calorimeter will add to produce an output pulse of sufficient amplitude to trigger the

calorimeter discriminator is proportional to the square of the beam intensity. The measured event rate, R^m, is therefore:

$$R^m = R^t(1+\alpha R^t) \tag{A-1}$$

where R^t is the true event rate and α is a constant proportional to the pulse width, i.e. of the order of 10^{-8} sec. when R^t is events per sec. The measured attenuation cross sections are obtained from the target in-out event rates via Eq. (13), i.e.

$$\sigma^m = [\ln R_o^m/R_i^m]/nx \tag{A-2}$$

where the subscripts "o" and "i" stand for target out and in respectively. Combining (A-1) and (A-2), expanding $(1+\alpha R^t)$ and dropping terms higher than the first order in R^t yields

$$\sigma^m \approx [\ln R_o^t/R_i^t + \ln(1+\alpha R_o^t - \alpha R_i^t)]/nx$$
$$= \sigma^c + \alpha(R_o^t - R_i^t)/nx \tag{A-3}$$

Let
$$R_o^t = (1+\epsilon)R_i^t \tag{A-4}$$

The targets used in this experiment typically attenuated the beam by a factor of 0.2 to 0.4, so that $\epsilon \approx 0.3$.

Combining (A-2) and (A-4) yields

$$\sigma^c = [\ln R_o^t/R_i^t]/nx = [\ln(1+\epsilon)]/nx$$
$$\approx (R_o^t - R_i^t)/R_i^t nx \tag{A-5}$$

and
$$\sigma^m \approx \sigma^c(1+\alpha R_i^t) \tag{A-6}$$

The αR term was typically 0.02.

APPENDIX III

BEAM RATE MEASUREMENT

The delay between $D1 \cdot \overline{A}$ and the 10% Cal which form the quantity Delayed Cal(10%)$\cdot D1 \cdot \overline{A}$ corresponds to one period of the Bevatron RF system. This means that the pulses from $D1 \cdot \overline{A}$ from one RF bunch arrive at the Delayed Cal(10%)$\cdot D1 \cdot \overline{A}$ "and" gate at the same time as the pulses from the calorimeter from the previous RF bunch. Since any two adjacent RF bunches are approximately the same, the Delayed Cal(10%)$\cdot D1 \cdot \overline{A}$ output is proportional to the accidentals rate in the normal Cal(10%)$\cdot D1 \cdot \overline{A}$.

The number of accidental coincidences in a twofold coincidence, g, expected per spill is proportional to

$$g \propto \int n^2(t) \cdot dt \qquad \text{(A-7)}$$

where n(t) is the beam intensity at time t. The number of true coincidences is proportional to

$$m \propto \int n(t) \cdot dt \qquad \text{(A-8)}$$

which is what the monitor measures. For a constant beam intensity the monitor measures the beam rate; however, in this experiment the beam was strongly modulated so the monitor was not a good indicator of the average instantaneous rate. To see that the Delayed Cal(10%)$\cdot D1 \cdot \overline{A}$ is a better indicator consider the three spill profiles below;

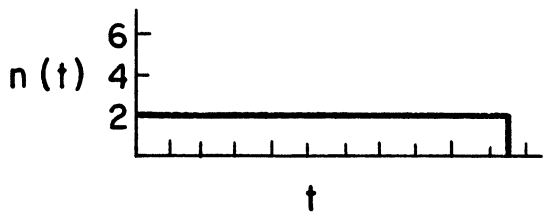

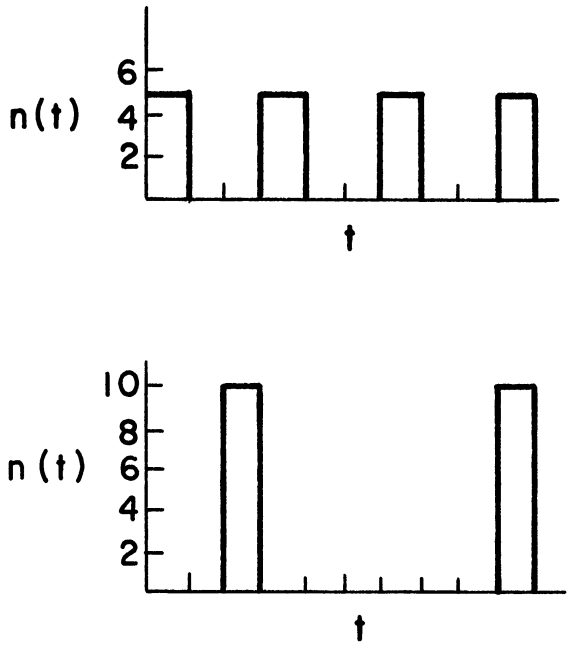

Since each contains the same number of particles the monitor would not differentiate between them. The Delayed Cal(10%)·Dl·$\overline{A}$ would rank them in the ratio 1:2.5:5, which is a reasonable estimate of the effective rates. The ratio Delayed Cal(10%)·Dl·$\overline{A}$/Cal(10%)·Dl·$\overline{A}$ is therefore a measure of the average rate.

APPENDIX IV

CALORIMETER BACKSCATTER

Another problem resulting from conversions in the body of the calorimeter was backscattering. There is a relatively large probability that a conversion taking place in the body of the calorimeter will produce a backward-going prong or γ-ray. If this radiation triggers the transmission counter an event in which the incident neutron did not interact in the converter will be incorrectly registered as a "signal" event. Backward-going radiation from "proper" conversions in the Fe converter plate can trigger the anticounter and a "signal" event will be incorrectly rejected. In order to evaluate these effects a series of beam attenuation measurements were made using the transmission counters alone, with and without the calorimeter located in the beam. The electronic logic for this study was the same as that shown in Fig. 6 except that the calorimeter was removed. The quantities scaled were $D1\cdot\overline{A}$, $D1\cdot D2\cdot\overline{A}$, $D1\cdot D2\cdot D3\cdot\overline{A}$, and $D1\cdot D2\cdot D3\cdot D4\cdot\overline{A}$. The $D1\cdot\overline{A}$ rate increased by 20% when the Calorimeter was physically at its normal location. The $D1\cdot D2\cdot\overline{A}$ rate increased by 2%, $D1\cdot D2\cdot D3\cdot\overline{A}$ rate increased by 1%, and $D1\cdot D2\cdot D3\cdot D4\cdot\overline{A}$ increased by 0.4%. The beam attenuation factors measured with and without the calorimeter present were, however, the same within statistics. Effects due to backscatter hitting the anticounters were completely

negligible because of the large separation between these counters and the converter plate.

APPENDIX V

GEOMETRIC RESPONSE FUNCTION FOR THE

TRANSMISSION COUNTERS

The geometric response function, $f_i(\theta)$, expresses the probability that a particle, scattered through an angle θ, will hit the ith transmission counter. Consider the following diagram of the beam and counter geometry.

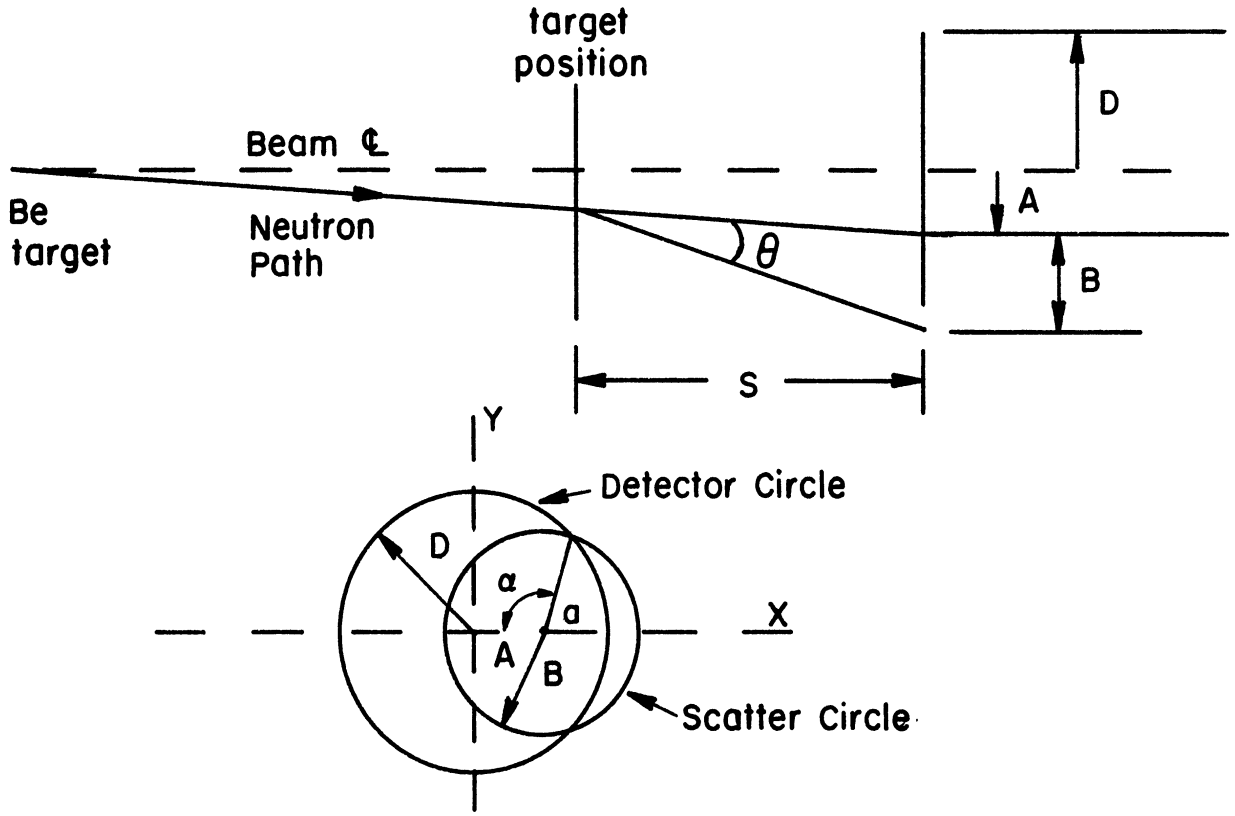

D is the radius of the ith transmission counter, a is the point where the neutron would hit if it had not been scattered through an angle θ, A is the distance between the center of the counter and a, S is the target-counter separation, and B is the radius of the "scatter circle" i.e. a circle with a radius equal to $\theta \cdot S$ centered at a. From

here on we will refer to a as the "image" point of the neutron. The probability that a neutron with an image at a will hit the detector if scattered through an angle θ is

$$P(\theta,A) \approx \alpha/\pi \qquad \text{(A-9)}$$

The detector circle and the scatter circle intersect at

$$x = (A^2 - B^2 + D^2)/2A \qquad \text{(A-10)}$$

Therefore

$$\cos(\alpha) = (A^2 + B^2 - D^2)/2A\cdot B \qquad \text{(A-11)}$$

and

$$P(\theta,A) = \frac{\cos^{-1}[(A^2 + B^2 - D^2)/2A\cdot B]}{\pi} \qquad \text{(A-12)}$$

If we assume that the beam has a constant intensity over its entire cross sectional area, the probability that a neutron will have an image point in an annulus of radius A and width dA is

$$P(A) = 2A\cdot dA/R^2 \qquad \text{(A-13)}$$

where R is the radius of the beam and $A \leq R$. We therefore get

$$f(\theta) = \begin{cases} 1, & \theta S \leq (D-R) \\ \int \cos^{-1}[(A^2 + B^2 - D^2)/2A\cdot B]\cdot 2A\cdot dA/\pi\cdot R^2, & (D-R) \leq \theta S \leq (D+R) \\ 0, & (D+R) \leq \theta S \end{cases} \qquad \text{(A-14)}$$

LIST OF REFERENCES

1. G.J. Igo, J.L. Friedes, H. Palevsky, R. Sutter, G. Bennett, W.D. Simpson, D.M. Corley, and R.L. Stearns, Nucl. Phys. B3, 181(1967).

2. K.J. Foley, R.S. Jones, S.J. Lindenbaum, W.A. Love, S. Ozaki, E.D. Platner, C.A. Quarles, and E.H. Wilson, Phys. Rev. Letters 19, 857(1967).

3. D.V. Bugg, D.C. Salter, G.H. Stafford, R.F. George, K.F. Riley, and R.J. Tapper, Phys. Rev. 146, 980 (1966).

4. G. Bellettini, G. Cocconi, A.N. Diddens, E. Lillethun, J.P. Scanlon, and A.M. Wetherell, Phys. Letters 19, 705(1966).

5. W. Galbraith, E.W. Jenkins, T.F. Kycia, B.A. Leontic, R.H. Phillips, A.L. Read, and R. Rubinstein, Phys. Rev. 138, 913(1965).

6. A.N. Diddens, E. Lillethun, G. Manning, A.E. Taylor, T.G. Walker, and A.M. Wetherell, Phys. Rev. Letters 9, 32(1962).

7. G. von Dardel, D.H. Frisch, R. Mermod, R.H. Milburn, P.H. Piroue, M. Vivargent, G. Weber, and K. Winter, Phys. Rev. Letters 5, 333(1960).

8. A. Ashmore, G. Cocconi, A.N. Diddens, and A.M. Wetherell, Phys. Rev. Letters 5, 576(1960).

9. M.J. Longo and B.J. Moyer, Phys. Rev. 125, 701(1962).

10. S.J. Lindenbaum, W.A. Love, J.A. Niederer, S. Ozaki, J.J. Russell, and L.C.L. Yuan, Phys. Rev. Letters 7, 185(1961).

11. G. Bellettini, G. Cocconi, A.N. Diddens, E. Lillethun, J. Pahl, J. Scanlon, J. Walters, A.M. Wetherell, and P. Zanella, Phys. Letters 14, 164(1965).

12. G. Bellettini, G. Cocconi, A.N. Diddens, E. Lillethun, G. Matthiae, J.P. Scanlon, and A.M. Wetherell, Phys. Letters 19, 341(1965).

13. J. Engler, K. Horn, J. König, F. Mönnig, P. Schludecker, H. Schopper, P. Sievers, and H. Ullrich, Phys. Letters 27B, 599(1968).

14. M.N. Kreisler, L.W. Jones, M.J. Longo, and J.R. O'Fallon, Phys. Rev. Letters 20, 468(1968).

15. V.P. Dzhelepov, V.I. Satarov, and B.M. Golovin, JETP 2, 349(1956).

16. N.E. Booth, G.W. Hutchinson, and B. Ledley, Proc. Phys. Soc. (London) 71, 293(1958).

17. H. Palevsky, J.L. Friedes, R.J. Sutter, R.E. Chrien, and H.R. Muether, "Proceeding of the Congres International de Physique Nucleaire 1964" edited by Mme. P. Gugenberger (Editions du Centre National de la Recherche Scientific, Paris, 1964) Vol. II, pp. 162.

18. V.A. Nedzel, Phys. Rev. 94, 174(1954).

19. A. Ashmore, R.G. Jarvis, D.S. Mather, and S.K. Sen, Proc. Phys. Soc. (London) A70, 745(1957).

20. M.N. Khachaturyan and V.S. Pantuyev, Nucl. Phys. 7, 80(1963).

21. J.H. Atkinson, W.N. Hess, V. Perez-mendez, and R. Wallace, Phys. Rev. 123, 1850(1961).

22. T. Coor, D.A. Hill, W.F. Hornyak, L.W. Smith, and G. Snow, Phys. Rev. 98, 1369(1955).

23. J. Engler, K. Horn, J. Konig, F. Monnig, P. Schludecker, H. Schopper, P. Sievers, and H. Ullrich, Phys. Letters 28B, 64(1964).

24. V.S. Pantuyev and M.N. Khachaturyan, JETP 15, 626 (1962).

25. G. Bellettini, G. Cocconi, A.N. Diddens, E. Lillethun, G. Matthiae, J.P. Scanlon, and A.M. Wetherell, Nucl. Phys. 79, 609(1965).

26. L.W. Jones, M.J. Longo, J.R. O'Fallon, and M.N. Kreisler, Phys. Letters 27B, 328(1968).

27. R.J. Glauber, Phys. Rev. 100, 242(1955).

28. M.J. Longo, "A Comparison of Experimental Data on Deuteron Screening Corrections with the Glauber Calculation", submitted to the Fourteenth International Conference on High Energy Physics, Vienna, August, 1968. (unpublished).

29. L. Van Hove, "Proceedings of the XIIIth International Conference on High-Energy Physics", (University of Cal. Press, Berkeley, Cal. 1967).

30. J. Pumplin and M. Ross, Phys. Rev. Letters 21, 1778 (1968).

31. M.N. Kreisler, S.L.A.C. Report # 66, Stanford Linear Accelerator Center, Stanford University, Stanford, Cal. (1966).

32. "200 Bev Accelerator Design Study" Vol. 1, Section XIII-1.3, page XIII-6, Lawrence Radiation Laboratory, University of Cal. Berkeley, Cal. (1965).

33. L.W. Jones, Tech. Report # 32, Dept. of Physics, University of Michigan, Ann Arbor, Michigan (1968).

34. V.S. Murzin, "Progress in Elementary Particles and Cosmic Ray Physics", (North-Holland Publishing Co. Amsterdam, The Netherlands, 1967), Vol. IX, pp. 245.

35. Edwin McLaughlin, Private Communication.

36. R.J. Corruccini, Pure and Applied Cryogenics, Vol. 5 (Pergamon Press, Oxford, London, New York, Paris, Braunschweig, Edinburgh, and Toronto, 1966) pp. 80.

37. E.C. Kerr, J. Am. Chem. Soc. 74, 824(1952).

38. C.F. Squire, Low Temperature Physics, (McGraw-Hill Book Co. Inc. New York, Toronto, and London, 1953) pp. 11.

39. K. Runge, Private Communication.

40. P. Sievers, Externer Bericht 3/68-12, Institute fur Experimentelle Kernphysik, Keinforschungszentrum Karlsruhe, Karlsruhe (1968).

41. M.L. Goldberger and K.M. Watson, Collision Theory, (John Wiley and Sons, Inc. New York, London, and Sydney, 1964) pp. 336.

42. R. Herman and R. Hofstadter, High-Energy Electron Scattering Tables, (Stanford University Press, Stanford, Cal. 1960) pp.62.